이학박사 학위논문

The effect of phosphoserine aminotransferase-1 dependent α-ketoglutarate fluctuation on timing of embryonic stem cell differentiation

Phosphoserine aminotransferase-1에 의한

α-ketoglutarate 조절이 배아줄기세포 분화시기에

끼치는 영향

2016년 8월

서울대학교 대학원

의과학과 의과학전공

황 인 영

ABSTRACT

The effect of phosphoserine aminotransferase-1 dependent α-ketoglutarate fluctuation on timing of embryonic stem cell differentiation

In-Young Hwang

Embryonic stem cells (ESCs) undergo coordinated epigenetic and metabolic changes to differentiate properly. However, the precise mechanisms by which these alterations are finely tuned at early stages of differentiation have not been identified. In this study, we demonstrate that phosphoserine aminotransferase 1 (Psat1), an Oct4/Sox2/Nanog target protein that regulates changes in α-ketoglutarate (α-KG), determines the fate of mESCs. Maintaining Psat1 level was essential for mESCs self-renewal and pluripotency. Moderate Psat1 knockdown mESCs had decreased DNA 5'-hydroxymethylation (5'-hmC) and increased histone methylation levels by downregulating permissive amounts of α-KG, ultimately accelerating differentiation. We found that intracellular α-KG transiently declined during differentiation and its disturbance by treatment with dimethyl-α-KG (dm-α-KG) delayed differentiation. Further, *in vivo* teratoma formation assay showed impaired pluripotency of Psat1 knockdown mESCs especially into

ectodermal lineage. Altogether, we reveal how Psat1 is regulated to maintain intracellular α-KG and the fate of mESCs.

Keywords: Stem cell, Metabolism, Epigenetics, Psat1 (Phosphoserine aminotransferase 1), α-ketoglutarate (α-KG)

Student number: 2009-21911

CONTENTS

LIST OF FIGURES

LIST OF TABLES

LIST OF ABBREVIATIONS

ESC	Embryonic stem cell
ICM	Inner cell mass
LIF	Leukemia inhibitory factor
2i	MEK/GSK3 inhibitors
Psat1	Phosphoserine aminotransferase 1
α-KG	α -ketoglutarate
5'-hmC	DNA 5'-hydroxymethylcytosine
dm-α-KG	Dimethyl-α-KG
Tet	Ten-eleven translocation family
JHDM	Jumonji C-domain-containing histone demethylase
HMT	Histone methyltransferase
Idh	Isocitrate dehydrogenase
Gls	Glutaminase
Glud1	Glutamate dehydrogenase 1
3-PG	3-phosphoglycerate
Got	Glutamate oxaloacetate transaminase
Gpt	Glutamate pyruvate transaminase

OAA	Oxaloacetate
Ccbl	Cysteine conjugate-beta lyase
Aadat	Aminoadipate transaminase
Abat	Aminobutyrate transaminase
Bcat	Branched chain aminotransferase
Tat	Tyrosine aminotranferase
OSN	Oct4, Sox2 and Nanog
PDB	Pubmed database
Atf4	Activating transcription factor 4
Phgdh	Phosphoglycerate dehydrogenase
Psph	Phosphoserine phosphatase
AP	Alkaline phosphatase
LC-MS	Liquid chromatography - mass spectrometry
H&E	Hematoxylin and eosin

I. INTRODUCTION

Mammalian development choreographed from a totipotent zygote to multiple lineages consisting of an organism. Following multiple cell divisions, totipotent is lost progressively specified into extraembryonic trophectoderm and ICM. When isolated from blastocyst, ICM cells can be directed toward either pluripotency or differentiation depending on media supplement (Figure 1) (Wu and Izpisua Belmonte, 2015). Murine ESCs grown with LIF/2i supplemented media, can maintain self-renewal and pluripotent states, and spontaneous differentiation can be triggered by subtracting LIF/2i from the media.

1-1 Master transcription factors in mESCS

Oct4/Sox2/Nanog are so-called master regulators in ESCs in that their roles in activation and recruit of much of pluripotent gene expression program (Whyte et al., 2013). Integrated transcription network constitute ESC characteristics, self-renewal and pluripotency (Figure 1). Pluripotent stem cells can differentiate into three germ layers, termed endoderm, mesoderm and ectoderm which can differentiate into all tissues consisting an organism. Dysregulation of these master transcription factors can impair pluripotency, self-renewal as well as proper differentiation. Thus, investigating the transcriptional regulatory network of these master transcription factors is indispensable.

1-2 Epigenetic changes during ESC differentiation

ESC differentiation is concomitant with dynamic epigenetic changes that are regulated precisely, such as DNA and histone modifications (Figure 1) (Lee et al., 2014; Liang and Zhang, 2013). The ten-eleven translocation (Tet) family enzymes

of DNA hydroxylases and Jumonji C-domain-containing histone demethylases (JHDMs) are α-KG/Fe^{2+}-dependent dioxygenases that use α-KG as a cofactor for their enzymatic activities, with pivotal functions in ESC self-renewal, pluripotency, and lineage specification (Figure 2) (Cimmino et al., 2011; Klose et al., 2006). Thus, their catalytic activities must be well orchestrated not only for maintaining pluripotency but also for proper differentiation.

1-3 Metabolism and epigenetic modifications

Recent studies have uncovered the direct links between metabolic and epigenetic changes in cancers and ESCs (Kaelin and McKnight, 2013; Yun et al., 2012; Zhang et al., 2012). For example, acetyl-coenzyme A is needed for nuclear histone acetylation and S-adenosylmethionine and S-adenosylhomocysteine are required for histone methylation to regulate gene expression affecting cell growth and differentiation (Mentch et al., 2015; Shyh-Chang et al., 2013; Sutendra et al., 2014). Intriguingly, mESCs exhibit a high-flux metabolic state for retaining their rapid cell growth and heavily rely on threonine catabolism to maintain pluripotent and self-renewal state. (Shyh-Chang et al., 2013; Wang et al., 2009). However, unique mechanism supporting mESC's chromatin landscape contributes to pluripotency maintenance and proper differentiation has not been identified.

1-4 Metabolic features of ESCs

ESCs, however, differ from somatic cells in that they harbor poorly developed mitochondria, forcing them to rely on glycolysis rather than oxidative phosphorylation (Figure 3) (Xu et al., 2013; Zhang et al., 2012). Blocking

glycolysis reduces the efficiency of somatic cell reprogramming, whereas enhancing glycolytic rates improves it (Folmes et al., 2011). Thus, glycolytic metabolites that compensate for low mitochondrial metabolite content in ESCs must be identified.

α-KG is an intermediate metabolite that is produced by isocitrate dehydrogenase during the tricarboxylic acid cycle in mitochondria. In addition, α-KG is also generated from glycolysis-branched amino acids synthesis pathways by transaminases, which transfer an amide group from glutamate, and also from glutamine metabolic process by Gls and Glud1 (DeBerardinis and Cheng, 2010; Locasale and Cantley, 2011; Wise and Thompson, 2010) (Figure 4). Based on the unique metabolic features of ESCs having low mitochondrial contents, we speculated a new mechanism to compensate α-KG demand for Tet and JHDM activities is needed.

In this study, we present evidence of Psat1-directed onset of differentiation through regulation of intracellular α-KG levels. Psat1-governed α-KG levels fine-tuned DNA 5'-hmC and histone H3K9 tri-methylation status in the regulatory regions of core transcription factors. Distorted intracellular α-KG level by knockdown of Psat1 resulted in early onset of stem cell differentiation. Up-regulation of intracellular α-KG by dm-α-KG delayed the onset of differentiation. Moreover, Psat1 knockdown mESCs lost differentiation potential into ectodermal lineages. Thus, this work has identified a novel mechanism by which metabolites shape epigenetic landscapes in determining the fate of mESCs.

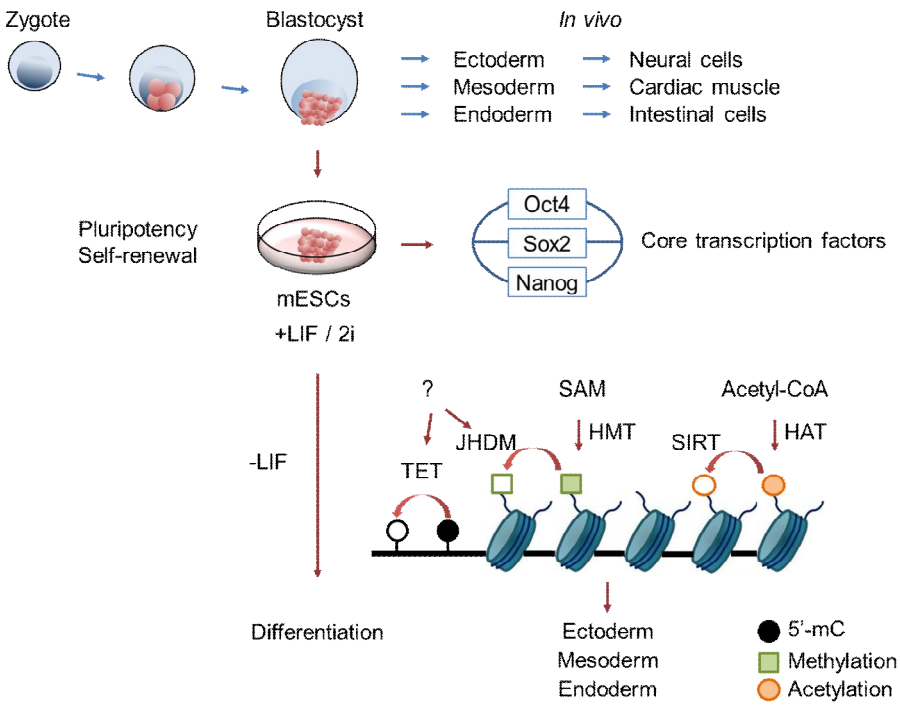

Figure 1. Dynamic epigenetic changes occur during ESC differentiation

mESCs are dissected from inner cell mass of blastocyst and can be maintained with LIF or 2i supplemented culture condition. Transcriptional network in mESC are regulated by Oct4/Sox2/Nanog. Differentiation can be triggered by subtracting LIF from growth media and various metabolite affect histone modifications and DNA methylation during lineage specification. For example, acetyl-CoA is needed for histone acetylation and SAM is a methyl donor for histone methylation. However, metabolites regulating histone methylation and DNA methylation in mESC are undiscovered.

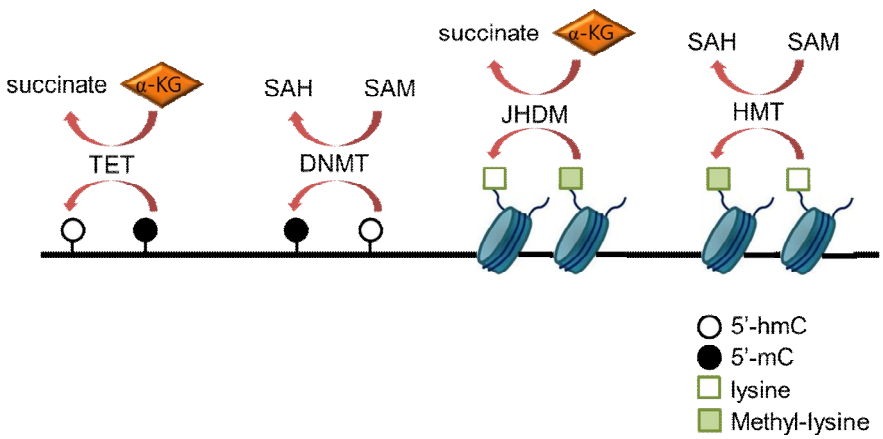

Figure 2. α-ketoglutarate (α-KG)/Fe^{2+}-dependent dioxygenases

Enzymes responsible for DNA methylation (DNMT) and histone methylation (HMT) use SAM as a methyl donor. Enzymes responsible for DNA demethylation and histone demethylation use α-KG as cofactor for their activities.

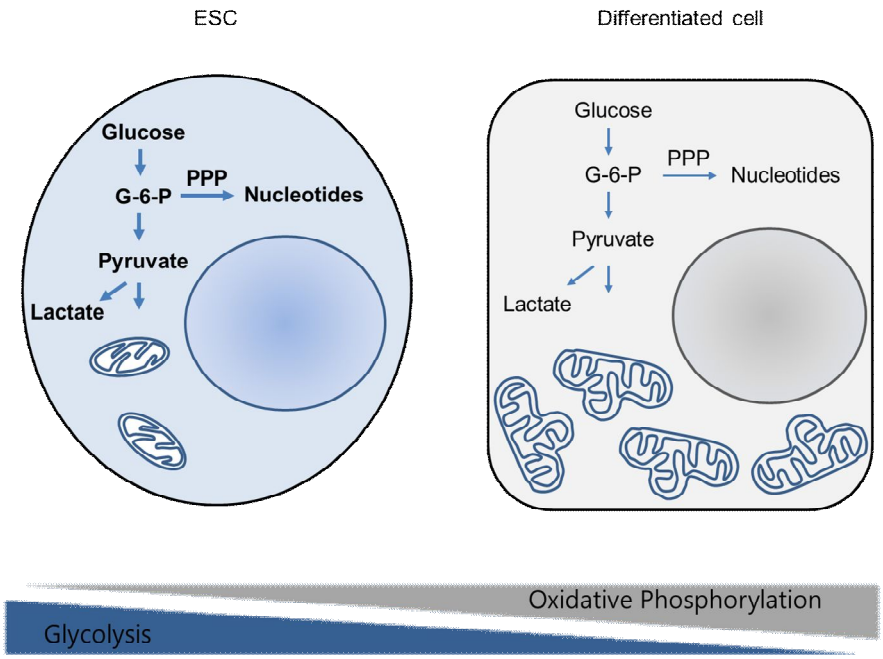

Figure 3. Unique metabolic states of ESCs

ESCs differ from somatic cells in that they harbor poorly developed mitochondria and thus low mitochondrial DNA and numbers. And they rely on glycolysis rather than oxidative phosphorylation. Pentose phosphate pathway and TCA cycle are activated than differentiated cells.

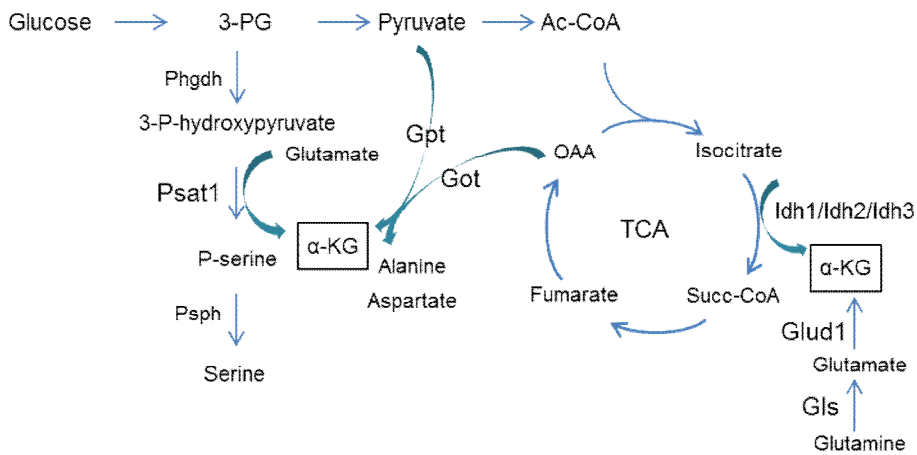

Figure 4. Diagram showing the major α-KG production pathways

α-KG is produced by isocitrate dehydrogenase during the tricarboxylic acid cycle and also from glycolysis-branched amino acids synthesis pathways - serine, alanine and aspartate biosynthesis- by transaminases which transfer an amide group from glutamate which is from glutamine metabolic process by Gls and Glud1

II. MATERIALS AND METHODS

2-1. Stable isotope labeling

Scr, Phgdh, Psat1 and Psph knockdown mESCs grown up to same confluency were changed with dialyzed FBS containing growth media for 24 hr. Then fresh media was changed 2hr before time counts for stabilization. 2mM of [U-^{13}C]-glutamine and 4.5 g/L of [U-^{13}C]-glucose (Cambridge Isotope Laboratories) containing media were used for measuring ^{13}C-α-KG and ^{13}C-serine respectively.

2-2. LC-MS

The extracted metabolites were injected with an injection volume of 5 μL. HPLC was performed on an Agilent 1100 Series liquid chromatography system equipped with a degasser (Agilent). The chromatographic separation was performed on a ZIC-pHILIC Polymeric Beads Peek Column (150 × 2.1 mm, 5 μm, Merck kGaA) at 35 °C, and the temperature of auto-sampler was set at 4 °C. For the solvent system, mobile phases A and B were distilled water with 10 mM ammonium carbonate (pH 9.1) and acetonitrile, respectively. The mobile phase was delivered at a flow-rate of 0.15 mL/min and the entire eluent was carried into a mass spectrometer. The linear gradient was as follows: 80% B at 0 min, 35% B at 10 min,5% B at 12 min, 5% B at 25 min, 80% B at 25.1 min, and 80% B at 35 min. An API 2000 Mass Spectrometer controlled by the Analyst 1.6 Software (AB/SCIEX) and equipped with an electrospray ionization (ESI) source was used in negative ion mode for multiple reaction monitoring (MRM). The operating conditions of the ass spectrometer were as follows:−4.5 kV of ion spray voltage, temperature of the heater (turbo) gas at 350 °C, and curtain gas (nitrogen),ion source gas 1 (nitrogen), and ion source gas 2 (nitrogen) at pressures of at 30, 40, and 80 psi, respectively. MRM was performed with the *m/z* value of the precursor

and fragment ions 106 > 60 for serine, 109 > 62 for ^{13}C-serine, 145 > 101 for α-KG 150 > 106 for ^{13}C-α-KG. The concentration of each metabolite was calculated mathematically from standard curve (5-100 μM) and normalized against total protein. The fraction of ^{13}C-serine and ^{13}C-α-KG in each cell lines were then calculated.

2-3. Metabolite extraction for LC-MS

4×10^6 cells of differentiated mESCs for indicated days were harvested and subjected to metabolite extraction. 4×10^6 cells of Scr, Psat1 knockdown and Flag-hPsat1 rescued Psat1 knockdown mESCs were changed with dialyzed FBS containing media, 24hr before metabolic extraction. After incubation with 2mM of [U-^{13}C]-glutamine and 4.5 g/L of [U-^{13}C]-glucose (Cambridge Isotope Laboratories) containing media for 0, 120 and 240 min, cells were harvested and extraction was followed using double phase methanol–chloroform extraction methods. Briefly, the cell pellets were re-suspended with the mixture of 400 μL methanol and 200 μL of chloroform. Three cycles of dipping into liquid nitrogen for 60 s, thawing at room temperature for 2 min and sonicating for 5 min were repeated. Then mixture of 200 μL chloroform and 200 μL of distilled water were added, and samples were centrifuged and the upper water phase was collected. Samples were dried with a centrifugal vacuum evaporator (Vision). The pellets were dissolved with HPLC-grade acetonitrile and water (1:1, v/v).

2-4. Histone purification

E14 mESCs were counted, and nuclear fractions were extracted using nuclear extraction buffer (10 mM Tris-Cl pH 7.4, 10 mM NaCl, 3 mM $MgCl_2$, 0.5 mM

dithiothreitol, 1 mM PMSF, Protease Inhibitor cocktail, 0.5% NP-40). Purified nuclear factions were boiled.

2-5. Hydroxymethylated DNA immunoprecipitation

Purified genomic DNA was diluted in Tris/EDTA buffer and sonicated. Then, 1 μg of genomic DNA and antibodies were diluted in IP buffer (0.01% SDS, 1.1% Triton X-100, 1.2 mM EDTA, 16.7 mM Tris-Cl pH 8.1, 167 mM NaCl) and incubated with agarose beads. The bound DNA was eluted, incubated with proteinase K, and purified by phenol/chloroform/isoamyl alcohol extraction.

2-6. Dot blot assay

Purified genomic DNA was denatured at 95°C for 10 min in 0.1 N NaOH, 0.2 M EDTA solution and cooled at 4°C. DNA was blotted onto nitrocellulose membranes and air-dried. Nitrocellulose membranes were baked at 80°C for 3 hr and blocked with 5% skim milk. 1 hr and western blot procedure was followed. 5'-mC (61255, Active Motif) and 5'-hmC (39769, Active motif) antibodies were used.

2-7. *In vivo* teratoma formation assay

100 μl of $2x10^6$ cells-matrigel mixture was injected into the subcutis of the SCID mice (Jackson Laboratories) used for transplantation. Observed routinely once a week for tumor growth, mice were sacrificed after 8 weeks. Excised tumors were fixed in 4% paraformaldehyde for overnight at 4°C. Paraffin embedded and section evaluation was done with H&E staining.

2-8. Histological analysis

Histological analysis of Paraffin embedded section was done with an unbiased pathologist.

2-9. Western blot analysis

Western blot was done as described (Hwang et al., 2012). Oct4 (sc-5279), Klf4 (sc-20691), Atf4 (sc-200), Tet3 (sc-139186) antibodies were purchased from Santa Cruz Biotechnology; Nanog (ab14959), Psat1 (ab-96136), Tet2 (ab94580), Jarid1c (ab-34718), Jmjd2c (ab-85454), H3 (ab-1791), H3K4me3 (ab8580), H3K9me3 (ab-8898), H3K36me3 (ab-9050-100) were purchased from Abcam; H3K27me3 (07-449), Tet1 (09-872), Jmjd1a (09-823) were from Millipore; Sox2 (MAB2018) was from R&D systems; Esrrb (PP-H6707-00) Perseus Proteomics; β-actin (A5441), Flag (F3165) Sigma-Aldrich; Jmjd2b (A301-478A) Bethyl-laboratories, Inc.

2-10. shRNA mediated knockdown

pLKO.1 lenti-viral vectors for shRNAs targeting mouse Psat1 were purchased from Sigma-Aldrich MISSON® library. shRNA sequences used in this study are as followed. shPsat1 #1 (TRCN 0000120417), #2 (TRCN 0000120419) and #3 (TRCN 0000120420)

2-11. Stable cell line generation

cDNAs were synthesized from RNAs of E14 mESCs and 293T cells. Amplified ORFs using PCR were introduced into Flag-pCAG vector. After transfection using Lipofectamine (Invitrogen) and Plus (Invitrogen) reagents, E14 mESCs were

selected with appropriate antibiotics (puromycin or blasticidin).

2-12. AP staining

AP staining (self-renewal) assay was done as described (Jang et al., 2012).

2-13. Genomic DNA preparation

E14 mESCs were lysed with 0.5 % SDS, 100mM NaCl, 50 mM Tris-Cl (pH 8.0) and 2mM EDTA. The lysates were incubated over-night with proteinase K and RNase. Then, phenol/ chloroform/ isoamyl alcohol purification was followed. Genomic DNAs were precipitated with sodium acetate (pH 5.2) and incubated at 65˚C to dissolve completely.

2-14. ChIP

ChIP assays were performed as described (Jang et al., 2012).

2-15. Quantitative real time PCR

Total RNAs were extracted from E14 mESCs, ZHBTc4 and 2TS22C cells with QIAzol (Qiazen). Extracted RNAs were synthesized into cDNAs by reverse-transcription with AMV Reverse Transcriptase for RT PCR analysis. RT PCR for cDNA were performed using EX Taq polymerase (Takara) and normalized to 18s rRNA. For ChIP and (h)MeDIP assays, SYBR® Green qPCR mix (Finnzymes, F-410) was used and the results are normalized to 1% input chromatin on CFX Connect Real-time PCR Detection System (Bio-Rad)

2-16. Cell culture

All ESCs in this study were cultured in feeder free condition on 0.1% gelatin-coated dishes. E14 mESCs were cultured in DMEM (Hyclone) or Knockout DMEM (Gibco) supplemented with 15% FBS (Gibco), 2 mM l-glutamine, 55 μM β-mercaptoethanol, 1% (v/v) non-essential amino acid, 100 U/ml penicillin and 100 μg/ml streptomycin, and 1000 U/ml ESGRO (Millipore). ZHBTc4 cells were provided by Hitoshi Niwa (RIKEN, Japan) and 2TS22C cells (Masui et al., 2007) were obtained from RIKEN CELL BANK. Before treating dm-α-KG, mESCs were changed with dialyzed FBS (Gibco) for indicated time and replenished with new dm-α-KG (Sigma-Aldrich) for every 12 hours. 2i culture was done as described previously (Carey et al., 2015).

2-17. Statistical analysis

Numerical values were expressed as the mean ± standard error of the mean (SEM) of three independent experiments. The statistical differences between two groups were analyzed by the two-tailed, unpaired Student's *t* test. The significant differences between two groups were declared as * $P \leq 0.05$ ** $P \leq 0.01$ *** $P \leq 0.001$.

Table 1. Real time PCR Primers for qPCR

Gene	Forward	Reverse
Oct4	AGGCAAGGGAGGTAGACAAGAGAA	AAATGATGAGTGACAGACAGGCCAGG
Sox2	GAGAGCAAGTAACTGGCAAGACCG	ATATCAACCTGCATGGACATTTTT
Nanog	ATGAAGTGCAAGCGGTGGCAGAAA	CCTGGTGGAGTCACAGAGTAGTTC
Klf4	ACAGGCGAGAAACCTTACCACTGT	GCCTCTTCATGTGTAAGGCAAGGT
Esrrb	AGTACAAGCGACGGCTGGAT	CCTAGTAGATTCGAGACGATCTTAGTCA
Bcat1	CCCATCGTACCTCTTTCACCC	GGGAGCGTGGGAATACGTG
Bcat2	CAGCCACACTAGGACAGGTCT	CAGCCTTGTTATTCCACTCCAC
Ccbl1	CGAAGGCTGGAAGGGATCG	GCGGTGAGAAGTCAGGGAA
Ccbl2	TTCAAAAACGCCAAACGAATCG	GATGACCAAAGCCTCTTGTGT
Got1	GCGCCTCCATCAGTCTTTG	ATTCATCTGTGCGGTACGCTC
Got2	GGACCTCCAGATCCCATCCT	GGTTTTCCGTTATCATCCCGGTA
Aadat	ATGAATTACTCACGGTTCCTCAC	AACATGCTCGGGTTTGGAGAT
Tat	TGCTGGATGTTCGCGTCAATA	CGGCTTCACCTTCATGTTGTC
Abat	CTGAACACAATCCAGAATGCAGA	GGTTGTAACCTATGGGCACAG
Gpt	TCCAGGCTTCAAGGAATGGAC	CAAGGCACGTTGCACGATG
Gpt2	AACCATTCACTGAGGTAATCCGA	GGGCTGTTTAGTAGGTTTGGGTA
Glud1	CCCAACTTCTTCAAGATGGTGG	AGAGGCTCAACACATGGTTGC
Gls1	CTACAGGATTGCGAACATCTGAT	ACACCATCTGACGTTGTCTGA
Gls2	CGTCCGGTACTACCTCGGT	TGTCCCTCTGCAATAGTGTAGAA
Idh1	ATGCAAGGAGATGAAATGACACG	GCATCACGATTCTCTATGCCTAA
Idh2	GGAGAAGCCGGTAGTGGAGAT	GGTCTGGTCACGGTTTGGAA
Idh3a	TGGGTGTCCAAGGTCTCTC	CTCCCACTGAATAGGTGCTTTG
Idh3b	TGGAGAGGTCTCGGAACATCT	AGCCTTGAACACTTCCTTGAC
Idh3g	GGTGCTGCAAAGGCAATGC	TATGCCGCCCACCATACTTAG
Psat1	CAGTGGAGCGCCAGAATAGAA	CCTGTGCCCCTTCAAGGAG
Phgdh	ATGGCCTTCGCAAATCTGC	AGTTCAGCTATCAGCTCCTCC
Psph	AGGAAGCTCTTCTGTTCAGCG	GAGCCTCTGGACTTGATCCC
Tet1	GCAGTGAACCCCGGAAAAC	AGAGCCATTGTAAACCCGTTG
Tet2	CTCCCATCAGCCATACAGAACC	CTGACTGTGCGTTTTATCCCT

Tet3	AGGCAGCTAAGCACCTCAG	GGCCCCGTAAGATGACACAG
Jarid1a	CCTGGCAGTAGGAGCAAAAG	AGAGTTCCTTTCCGTTGTCTCA
Jmjd1a	CAGTCTTCGGCTTTCCCTTAC	AACCAACAAGGTTCTTGTCACC
Jmjd2b	GCTTTAACTGCGCTGAGTCC	CGTCCATGGAGATCTTGACC
Jmjd2c	TGGCACCTATTTATGGAGCAG	TCTTCAACCACATCCAAGACTG
Utx	AATGCACCACCTCCAGTAGAAC	CAGCATTAGTTTCTGTGCTGGA
Jmjd3	GTGAAAGGGAAATTCCGAGAG	AATAGATGCTGGGGGTAGGG

Table 2. Real time PCR primers for ChIP

	Forward	Reverse
Oct4	CTTGAACTGTGGTGGAGAGTGCTG	TAAGGAAGGGCTAGGACGAGAGG
Sox2	CCCATTTATTCCCTGACAGC	CTCTTCTTTCTCCCAGCCCTA
Nanog	CTCCTACCCTACCCACCCCCTATT	TTAGATCAGAGGATGCCCCCTAAG
Klf4	CGATTGTGCTGGATTGCTTT	AACGCACTCAGGTGCAACAT
Esrrb	CGGCTGGTATCACCTGATTTAC	GGCCACCTCCAAATCCAAA
Psat1 pou5f1:: sox2 Motif	TCACAGCTGGCTCTTTGGAC	CAGTCATAGGCTGTTGGCGT
Psat1 CRE site	GGCAGGACCAAAAAGACACTG	ACAGAACGGGACCGGTAGAG

Table 3. Real time PCR primers for hMeDIP

	Forward	Reverse
Oct4	GGAGGTGCAATGGCTGTCTTGTCC	CTGCCTTGGGTCACCTTACACCTCAC
Sox2	GGAGGCTGGTGTAAGGTGGT	CCAAGCTGGATCACTCCTCA
Nanog	GTTGGTGTGGCTCAGAGGTG	CCACCATTGTTACCACTGCC
Klf4	CGATTGTGCTGGATTGCTTT	AACGCACTCAGGTGCAACAT
Esrrb	ATTGTCTTCCCAGCTCCCAC	GGTCTCAAGCAAAACAGCCA

Ⅲ. RESULTS

3-1. Psat1 Is Regulated by Core Transcription Factors in mESCs

Using Gene Ontology gene sets, we selected enzymes that were involved in α-KG production, based on their molecular function (Table 4).

To identify enzymes mediating α-KG synthesis in mESCs, we established 3 criteria: 1) high expression in mESCs, 2) downregulation on differentiation, and 3) direct regulation by Oct4, Sox2, and Nanog (OSN). Publically available RNA-sequencing data were analyzed (Wamstad et al., 2012; Xiao et al., 2012), and Psat1, Bcat2, and Gpt2 were highly expressed in mESCs and declined rapidly on differentiation (Figure 4 and 5). Next, 3 independent chromatin immunoprecipitation (ChIP) sequencing datasets were used to determine the occupancy of OSN in the promoter and enhancer regions of these enzymes (Chen et al., 2008; Marson et al., 2008; Whyte et al., 2013). Psat1, Glud1, and Idh2 had regions with all three OSN occupancy (Figure 6 and Table 5). Combining the RNA-sequencing and ChIP-sequencing datasets, Psat1 was the only factor to meet all 3 criteria. The expression pattern of Psat1 was confirmed using differentiation triggered mESCs by subtracting leukemia inhibitory factor (LIF) from growth media. The Psat1 level fell on withdrawal of LIF, as expected (Figure 7). Notably, Psat1 protein levels fluctuated on day 4 of LIF withdrawal, which we speculated resulted from up-regulation of activating transcription factor 4 (Atf4) in that its role in regulating Psat1 and lineage specification (DeNicola et al., 2015; Jixiu Shan, 2013; Ye et al., 2012). knockdown of Atf4 abolished the elevation in Psat1 on day 4 of LIF removal (Figure 8A and 8B).

GO:0006103 2-oxoglutarate metabolic process:	Got1
	Got2
	Aadat
	Gpt2
	Tat
	Idh1
	Idh2
	Ccbl2
	Idh3b
	Idh1
	Idh3g
GO:0008483: Transaminase activity	Bcat1
	Bcat2
	Got1
	Got2
	Aadat
	Tat
	Ccbl1
	Ccbl2
	Gpt1
	Gpt2
	Psat1
GO:0004359 Glutaminase activity	Gls1
	Gls2
GO:0004352 Glutaminase dehydrogenase activity:	Glud1
	Glud2

Table 4. List of enzymes related to α-KG generation

Gene Ontology of enzymes related to α-KG generation are shown according to their molecular function

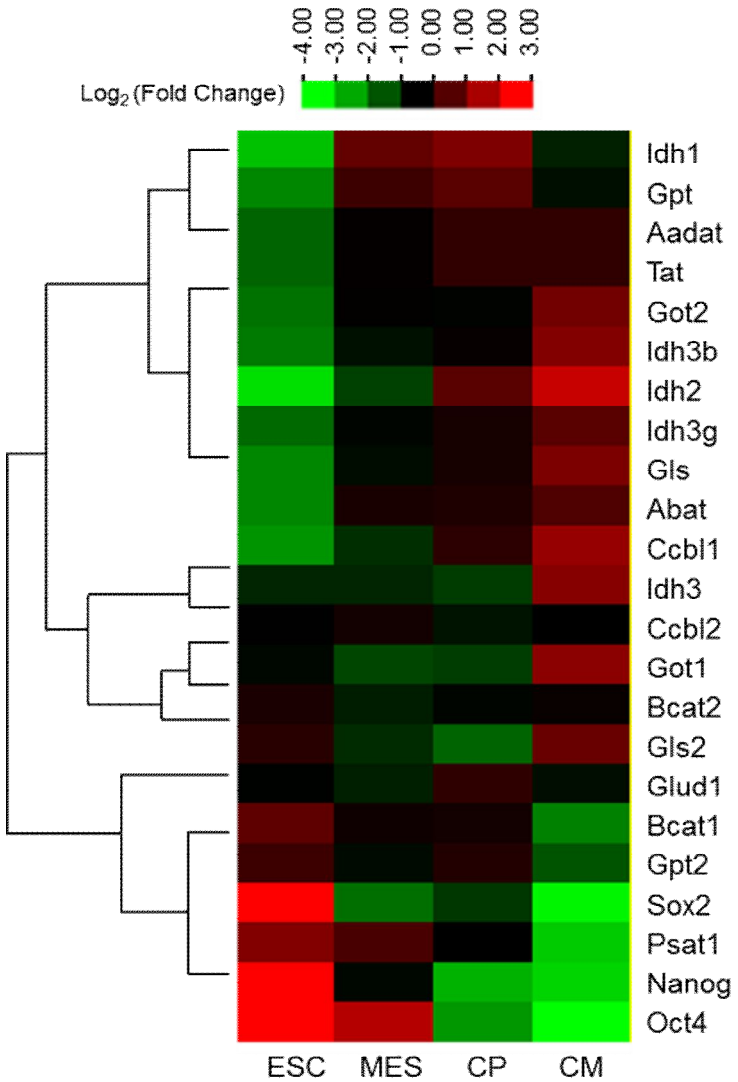

Figure 5. Expression levels of α-KG synthesis related enzymes during cardiomyocyte differentiation

The raw RNA-sequencing data from Wamstad et al., 2012 were processed and Read per kilobase per million mapped reads was transformed into $\log_2$ values using Spearman rank correlation. Mesodermal cell (MES), cardiac precursor (CP), cardiac myocyte (CM).

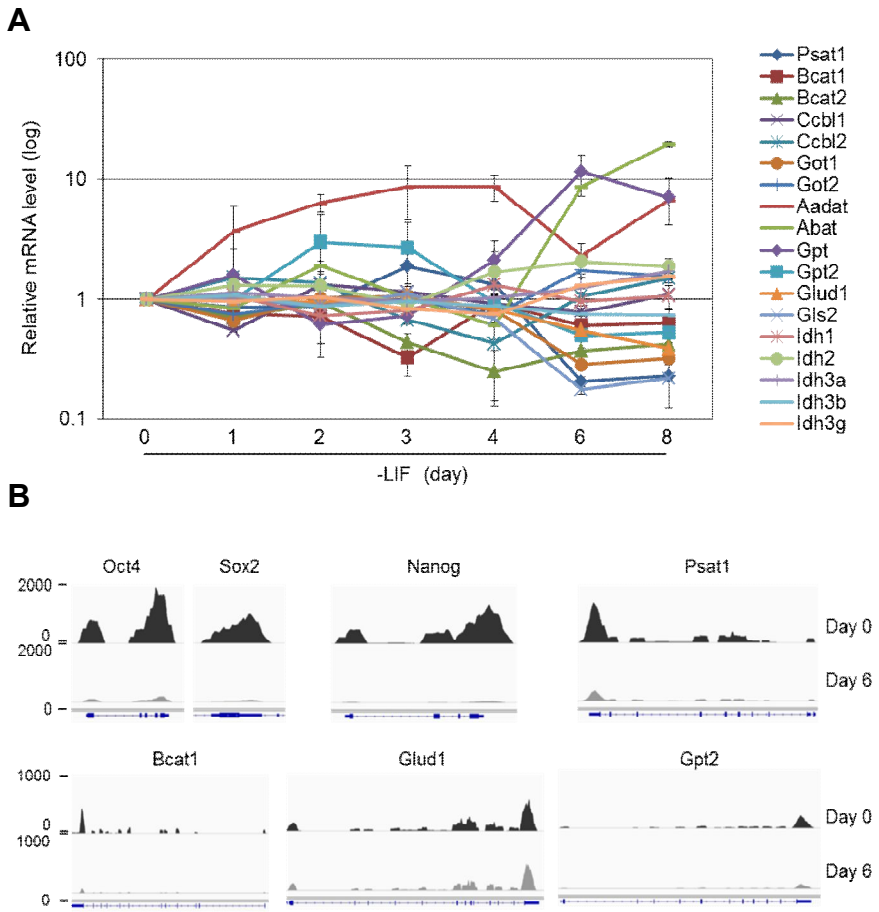

Figure 6. Expression levels of α-KG synthesis related enzymes in ESCs

(A) mRNA levels of candidate enzymes are confirmed after LIF subtraction for indicated days (n=3). Data are presented as means ±SEM. (B) Expression levels of OSN and 4 candidate enzymes are visualized using Integrative Genomic Viewer (IGV) program from RNA-sequencing data. (PDB: GSE36114).

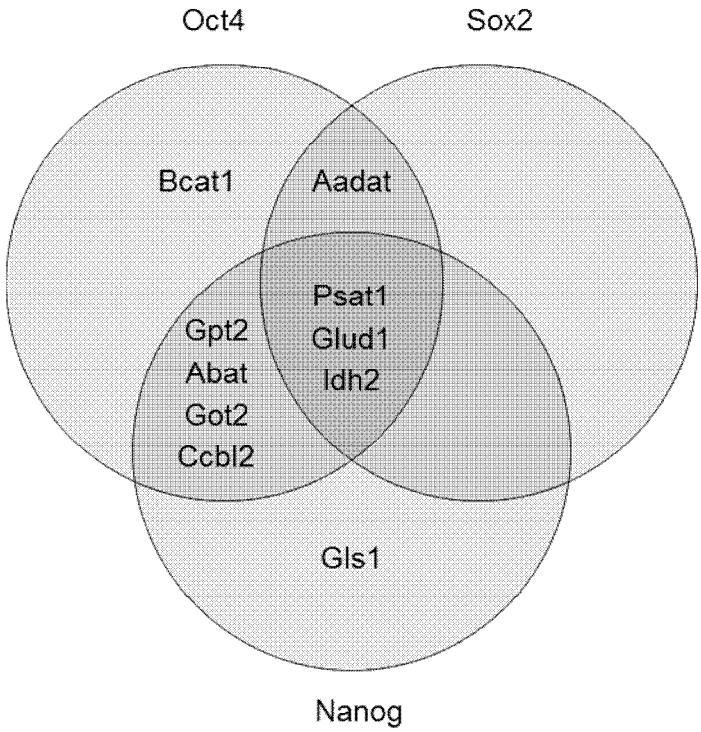

Figure 7. Venn diagram showing enzymes occupied by OSN

Three independent ChIP-sequencing datasets from Pubmed data base are used. The raw data files are processed in house by model-based analysis for ChIP-sequencing technology. Only Psat1, Glud1 and Idh2 are bound by Oct4/Sox2/Nanog proteins.

	PDB: GSE44288			PDB: GSE11432			PDB: GSE11724		
	Oct4	Sox2	Nanog	Oct4	Sox2	Nanog	Oct4	Sox2	Nanog
Psat1	○	○	○	○	○	○	○	○	○
Idh2	○	○	○	○	○	○	○	○	○
Glud1	○	○	○	○	○	○	○	○	○
Aadat	○	○	○	○	○	X	○	○	○
Got2	○	X	○	○	○	○	○	○	○
Abat	○	X	○	○	○	○	○	○	○
Gpt2	○	X	○	X	○	○	○	○	○
Ccbl2	○	X	○	○	X	○	○	X	○
Bcat1	○	○	○	○	X	X	○	○	○
Gls	X	○	○	X	○	○	○	X	○
Got1	○	○	○	○	X	X	X	○	X

Table 5. Three independent ChIP-sequencing data sets with OSN

Detailed information of OSN binding to α-KG production related enzymes are presented. Enzymes with OSN bindings are shown only. Accession numbers for Pubmed data bases are shown.

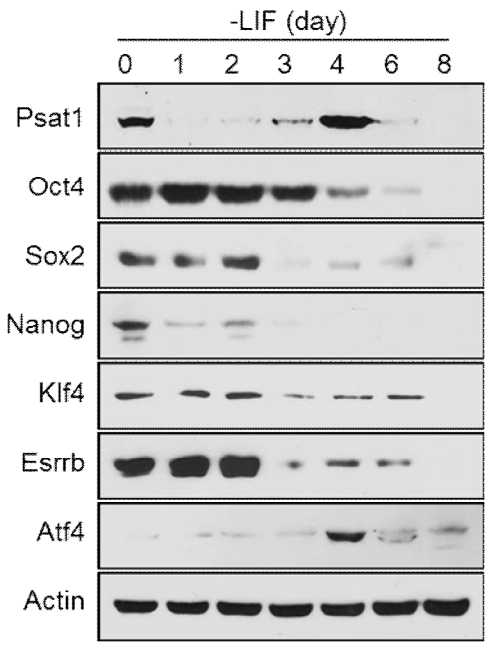

Figure 8. Expression levels of Psat1 on withdrawal of LIF

Western blots of Psat1 and core transcription factors on LIF withdrawal for indicated days. Psat1 protein level decreased on early time point of differentiation. This experiment was repeated at least three times with similar results. The most representative blots are shown.

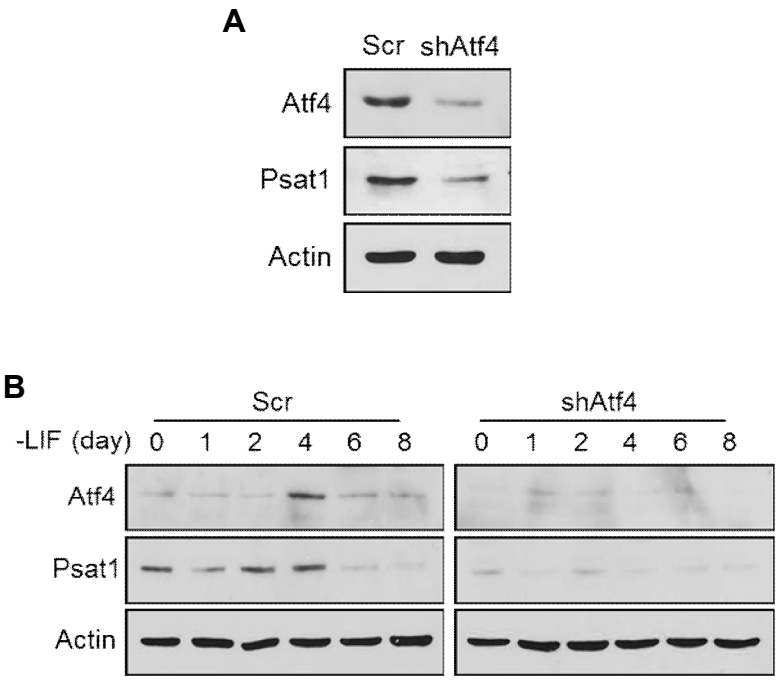

Figure 9. Psat1 is regulated by Atf4 on late time point of differentiation.

(A) Western blot of Atf4 knockdown is shown. (B) mESCs are triggered to differentiate by LIF removal and protein levels of Atf4 and Psat1 are shown. Repeated three times, and the most representative data are shown.

Next, we searched the JASPAR database to find binding motifs for Oct4 and Sox2 in the *Psat1* enhancer (Mathelier et al., 2014). We observed a *Oct4::Sox2* motif in the *Psat1* enhancer and we performed ChIP on these region (Figure 9A and 9B). Robust binding of OSN was detected at these regions and two days of LIF removal was sufficient to release OSN, consistent with the Psat1 expression pattern in Figure 6. To confirm that *Psat1* is regulated by Atf4 after OSN is released, we performed ChIP of the canonical *Atf4* binding site in the *Psat1* enhancer. Atf4 binding to the canonical *Atf4* binding site increased on day 4 after LIF withdrawal (Figure 10).

The direct transcriptional regulation of Psat1 by Oct4 and Sox2 was verified further in genetically engineered ZHBTc4 and 2TS22C cells (Masui et al., 2007). Psat1 protein and mRNA were down-regulated when doxycycline was used to deplete Oct4 and Sox2 in ZHBTc4 and 2TS22C cells, respectively (Figure 11A and 11B). Psat1 level recovered when Flag-Oct4 and Flag-Sox2 were introduced.

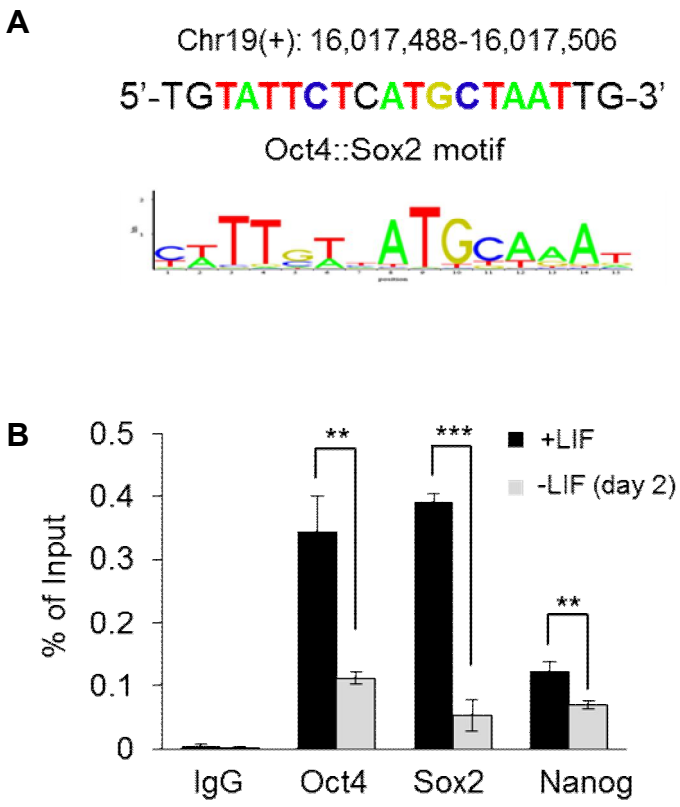

Figure 10. OSN binds on Psat1 enhancer

(A) Predicted sequences of *Oct4::Sox2* consensus motif on *Psat1* enhancer are shown (upper panel). (B) OSN binding to this motif is shown by ChIP assay with and without LIF for the indicated day (right panel) OSN binding to *Oct4::Sox2* motif decreased after withdrawal of LIF (n=3).

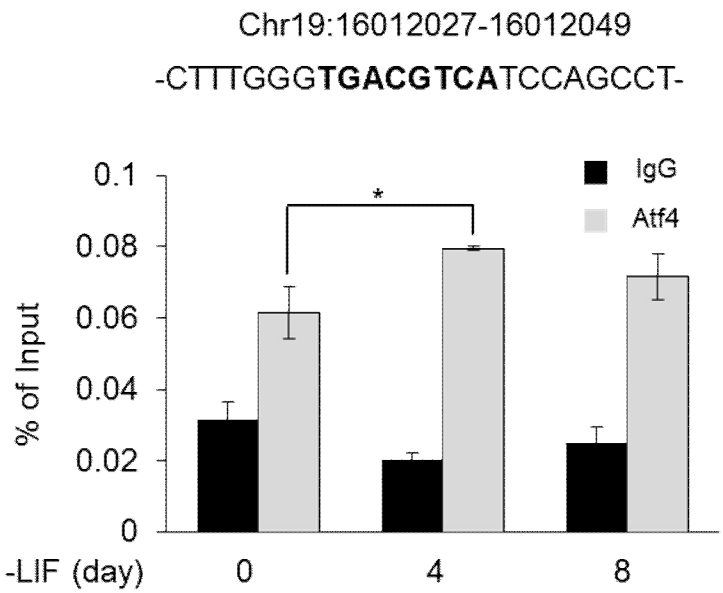

Figure 11. Atf4 binds on Psat1 enhancer

ChIP assay showing Atf4 binding on *Psat1* enhancer (n=3). Atf4 binding to Atf4 consensus sequence in *Psat1* enhancer are shown (up). Atf4 binding decreases on Day 4 of LIF withdrawal. Data are presented as means ±SEM. * $P \leq 0.05$.

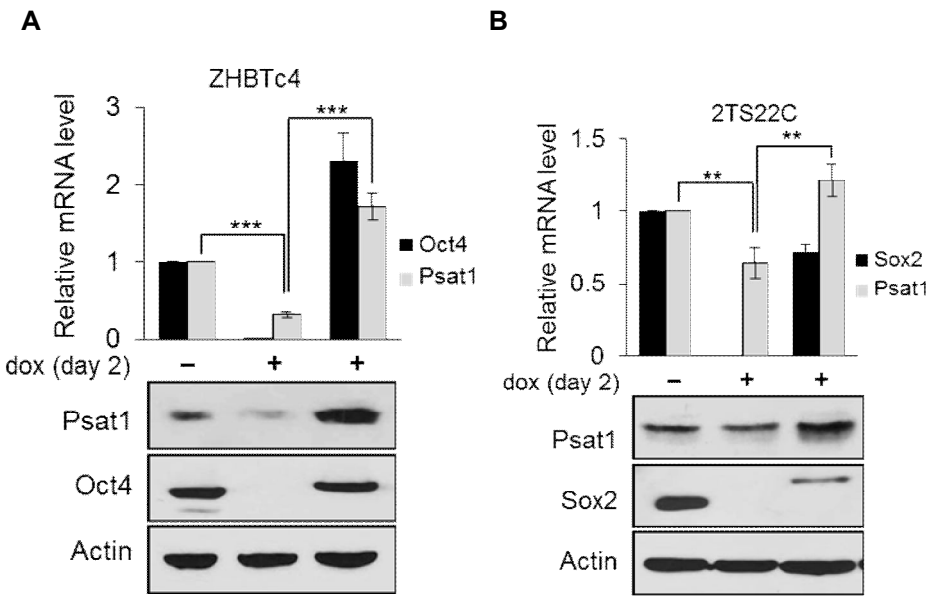

Figure 12. Direct regulation of Psat1 level by Oct4 and Sox2

(A) and (B) mRNA and protein levels of Psat1 and Oct4 in ZHBTc4 cells(A) and Psat1 and Sox2 in 2TS22C cells (B). Oct4 and Sox2 are depleted on treatment of dox and lowered Psat1 level. Ectopic Oct4 and Sox2 expression restored the Psat1 level (n=3). Data are presented as means ± SEM. ** $P \leq 0.01$ *** $P \leq 0.001$

Interestingly, it has been reported that naïve mESCs rely on α-KG to maintain pluripotency (Carey et al., 2015). Thus we confirmed whether Psat1 is also regulated by OSN after glycogen synthase kinase 3β and mitogen-activated protein kinase inhibitors (2i) treatment which mimics naïve state of mESCs. We found OSN binding on *Psat1* enhancer after 2i treatment (Figure 10A). Moreover, we processed publically available ChIP-sequencing data, and also OSN binding were found on Psat1 enhancer after 2i treatment (Figure 12A and 12B) (Galonska et al., 2015). Then we detected protein and mRNA levels of Psat1 and found increment of Psat1 level after 2i treatment (Figure 12C and 12D).

Psat1 is responsible for the second reaction in *de novo* serine biosynthesis which converts 3-phosphohydroxypyruvate to 3-phosphoserine by coupled conversion of glutamate to α-KG. This pathway consists of phosphoglycerate dehydrogenase (Phgdh) and phosphoserine phosphatase (Psph) for the first and the third enzyme respectively (Figure 2). We examined whether these two enzymes are also regulated by OSN in mESCs. We could not find OSN binding on genomic regions of *Phgdh* and *Psph* from ChIP-sequencing data from both S/L and 2i culture conditions (Figure 13A). And only Psat1 was found to be regulated by Oct4 after performing ChIP assay with Oct4 and its mRNA depletion using ZHBTc4 cells (Figure 11A and 11B). Based on these findings, we conclude that Psat1 is a direct target of core transcription factors in mESCs.

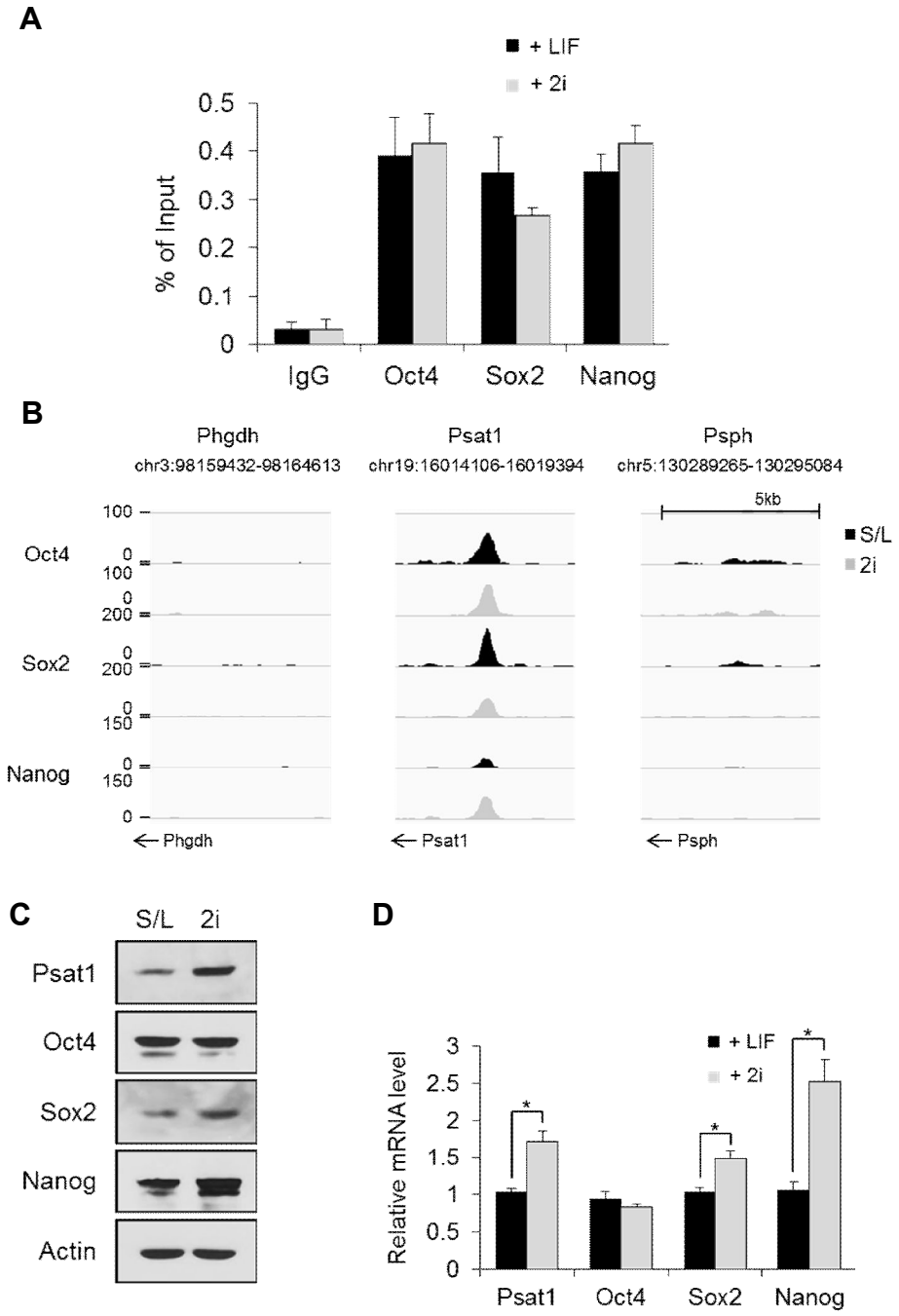
A
+ LIF
+ 2i
% of Input
0.5
0.4
0.3
0.2
0.1
0
IgG
Oct4
Sox2
Nanog
B
Phgdh
chr3:98159432-98164613
Psat1
chr19:16014106-16019394
Psph
chr5:130289265-130295084
5kb
S/L
2i
Oct4
Sox2
Nanog
100
0
100
0
200
0
200
0
150
0
150
0
Phgdh
Psat1
Psph
C
S/L
2i
Psat1
Oct4
Sox2
Nanog
Actin
D
+ LIF
+ 2i
Relative mRNA level
3
2.5
2
1.5
1
0.5
0
*
*
*
Psat1
Oct4
Sox2
Nanog

Figure 13. OSN also regulates Psat1 in 2i culture condition

(A) OSN binding in S/L condition was compared to 2i culture condition (n=3). (B) OSN bindings on indicated genomic regions are shown by IGV. Public ChIP sequencing data were processed (GSE 56312). Only Psat1 enhancer is bound by OSN, but not Phgdh and Psph, the other two enzymes in serine de novo biosynthesis pathway. (C) Protein and (D) mRNA levels of Psat1 and core transcription factor in S/L and 2i condition (n=3). Data are presented as means ± SEM. * $P \leq 0.05$

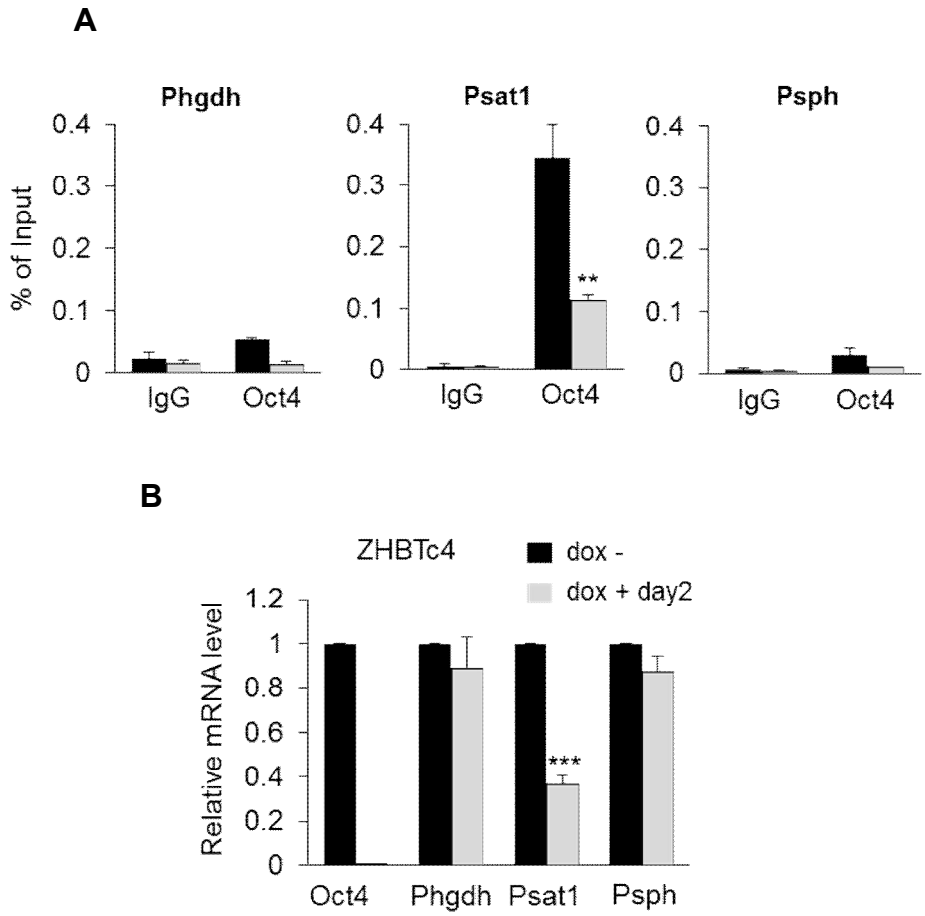

Figure 14. Phgdh and Psph are not regulated by OSN

(A) ChIP assays were done to verify Oct4 binding on the genomic regions. Only Psat1 enhancer is bound by Oct4. (B) mRNA levels of serine biosynthesis enzymes in ZHBTc4 cells after dox treatment (n=3). Psat1 mRNA level is lowered after treatment of Dox to deplete Oct4. Data are presented as means ±SEM. ** $P \leq 0.01$

3-2 Psat1 Regulates Intracellular α-KG Levels in mESCs

Although Psat1 is a glycolysis-branched transaminase that mediates the production of α-KG, whether it actually regulates intracellular α-KG levels in mESCs is unknown. Thus we introduced Psat1 shRNAs into mESCs to knockdown endogenous Psat1 (Figure 14A and 14B). Moderate Psat1 knockdown clone 2 had no effect on self-renewal, but severe Psat1 knockdown clone 3 failed to maintain self-renewal and pluripotency, as evidenced by the alkaline phosphatase (AP) staining (Figure 15A). Ectopic expression of shRNA resistant Flag-human PSAT1 (hPSAT1) had more AP positive colonies in clone 3, indicating specificity of Psat1 shRNA. Psat1 knockdown clones downregulated Sox2, Nanog, Klf4, and Esrrb (Figure 15B). Oct4 levels, however, declined significantly only with severe Psat1 knockdown clone 3 (Figure 14A). To examine whether Psat1 knockdown reduced intracellular α-KG, we performed liquid chromatography-mass spectrometry (LC-MS). Intriguingly, both Psat1 knockdown clones 2 and 3 were sufficient to reduce intracellular α-KG content and it was recovered when Flag-hPSAT1 was introduced (Figure 16).

Next, we tested whether the failure of self-renewal and pluripotency maintenance in severe Psat1 knockdown clone 3 was caused by reduced level of intracellular α-KG using cell membrane-permeable compound dm-α-KG. We treated dm-α-KG in dose dependent manner to choose appropriate concentration to avoid cell growth from being affected (Figure 17A). Because dm-α-KG is consumable, we measured the protein levels of core pluripotency factors for various periods. Treatment with dm-α-KG for 4–16 hr effected the increase in core transcription factors (Figure 17B). Then, we treated dm-α-KG on Psat1 knockdown clone 3 cells continuously

after shRNA introduction. We found more AP-positive colonies in clone 3 and core pluripotency factors levels were recovered after dm-α-KG treatment (Figure 18A, 18B and 18C).

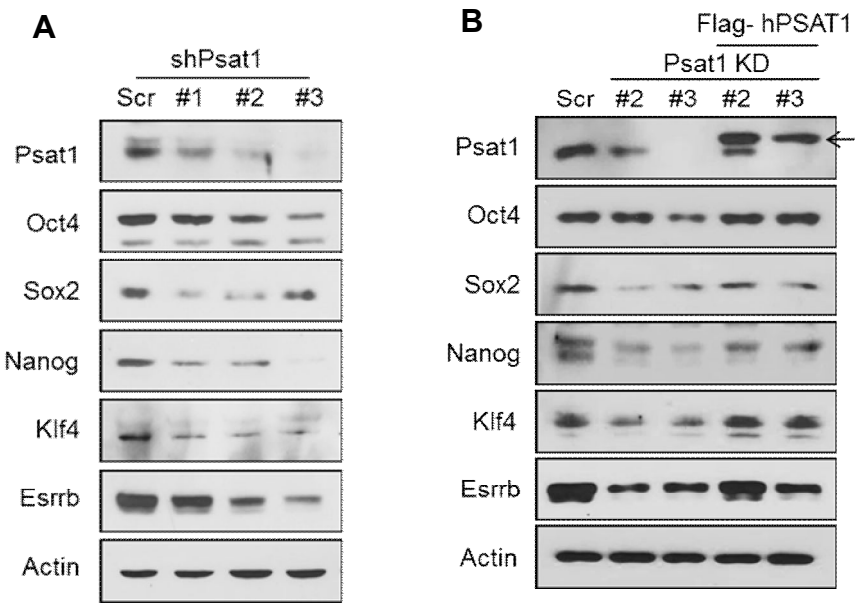

Figure 15. Psat1 knockdown mESCs have reduced core transcription factors

(A) Several Psat1 knockdown mESCs and protein levels of core transcription factors are shown by western blot. Psat1 knockdown reduced core transcription factors. (B) Western blots of core transcription factors in Psat1 knockdown and human PSAT1 rescued clones. hPSAT1 restored the level of core transcription factors. Arrow indicates Flag-hPSAT1.

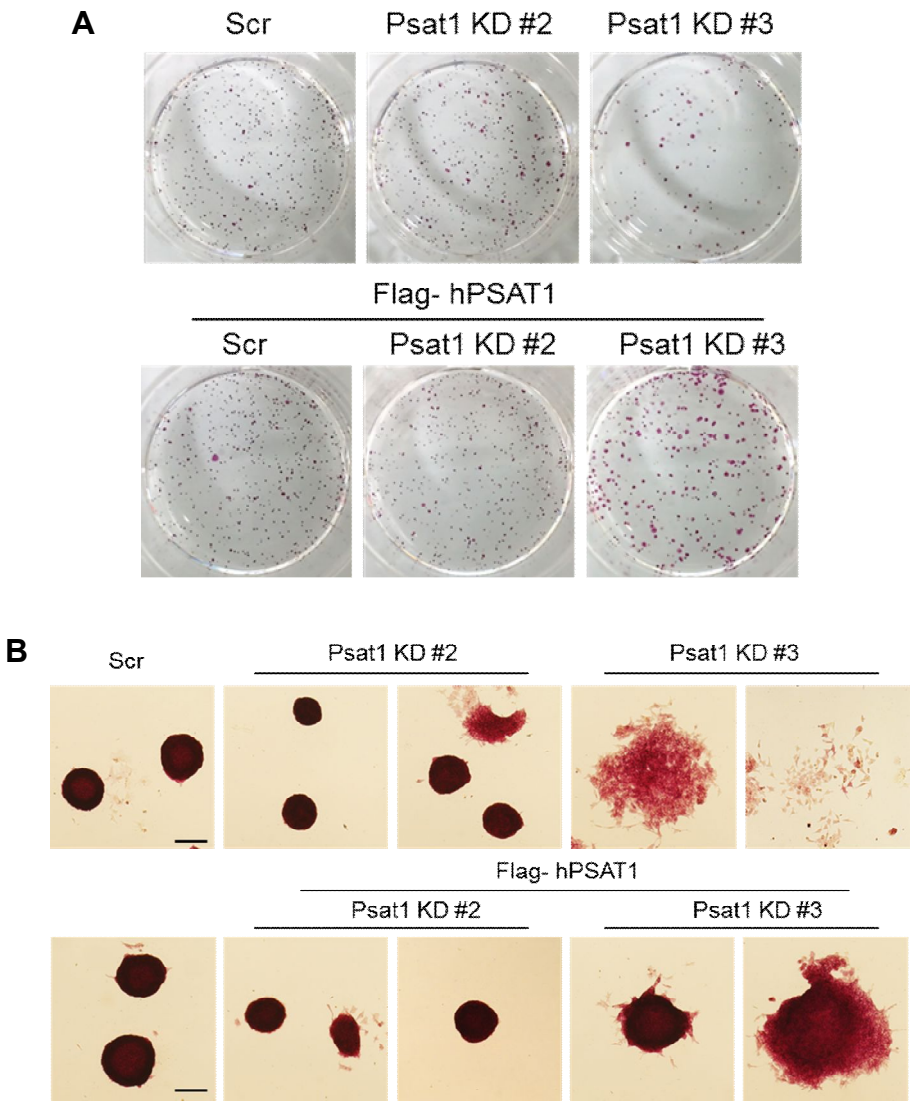

Figure 16. Psat1 level is essential for maintaining self-renewal states

(A) AP staining of Psat1 knockdown clones 2 and 3, and Flag-hPsat1 rescued mESCs and (B) their enlargement. Severe knockdown of Psat1 impaired self-renewal of mESCs and hPSAT1 recued self-renewal defects. Scale bar represents 500μm.

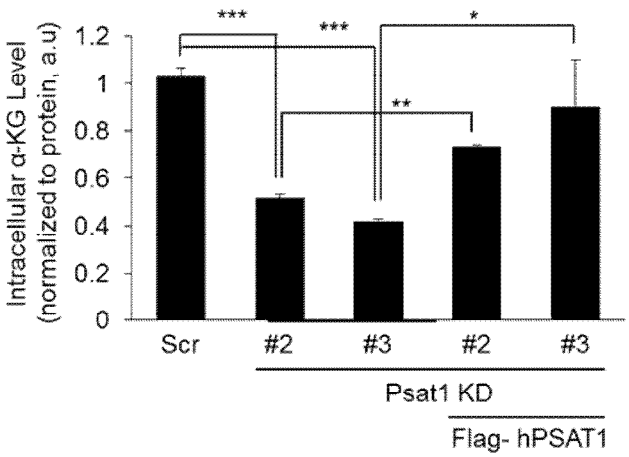

Figure 17. Psat1 knockdown mESCs have reduced intracellular α-KG level

Intracellular α-KG level was measured in Psat1 knockdown clones and rescued cell lines using LC-MS. Reduced intracellular α-KG was restored after ectopic hPSAT1 expression. Data are presented relative to Scr cells (n=3). a.u. arbitrary units * $P \leq 0.05$ ** $P \leq 0.01$ *** $P \leq 0.001$.

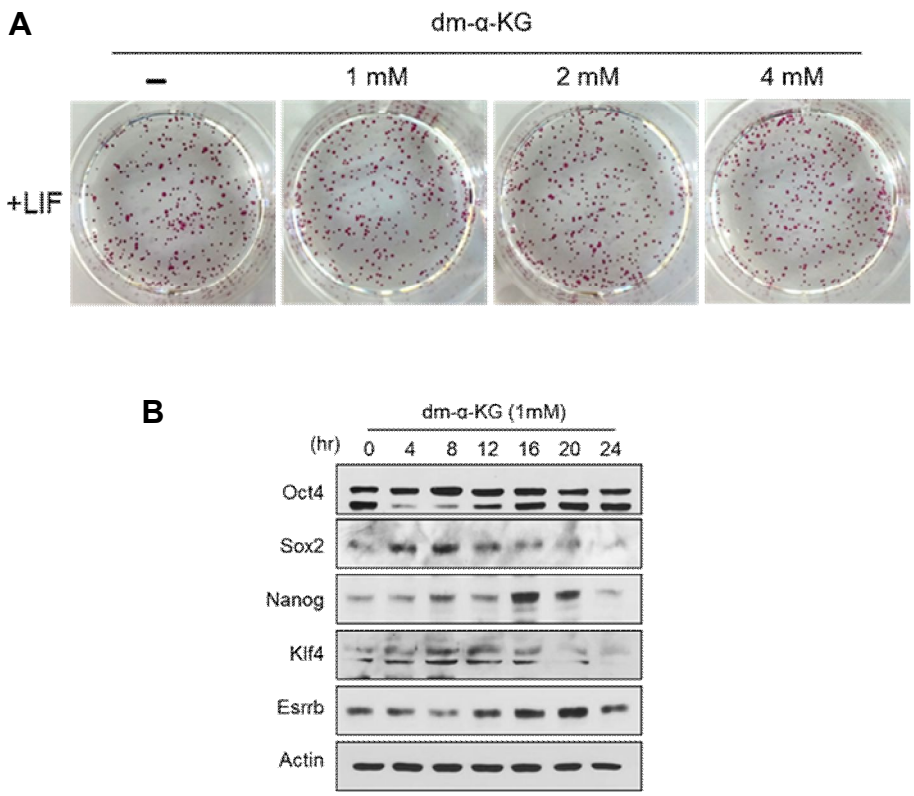

Figure 18. Effect of dm-α-KG treatment on mESCs

(A) AP staining of dose-dependent dm-α-KG treated mESCs. AP staining is repeated three times. (B) Core transcription factors protein level changed during various periods of dm-α-KG treatment. Core transcription factors protein level fluctuated between 4hr-20hr after dm-α-KG treatment. This experiment was repeated two times each for normal FBS and dialyzed FBS culture condition.

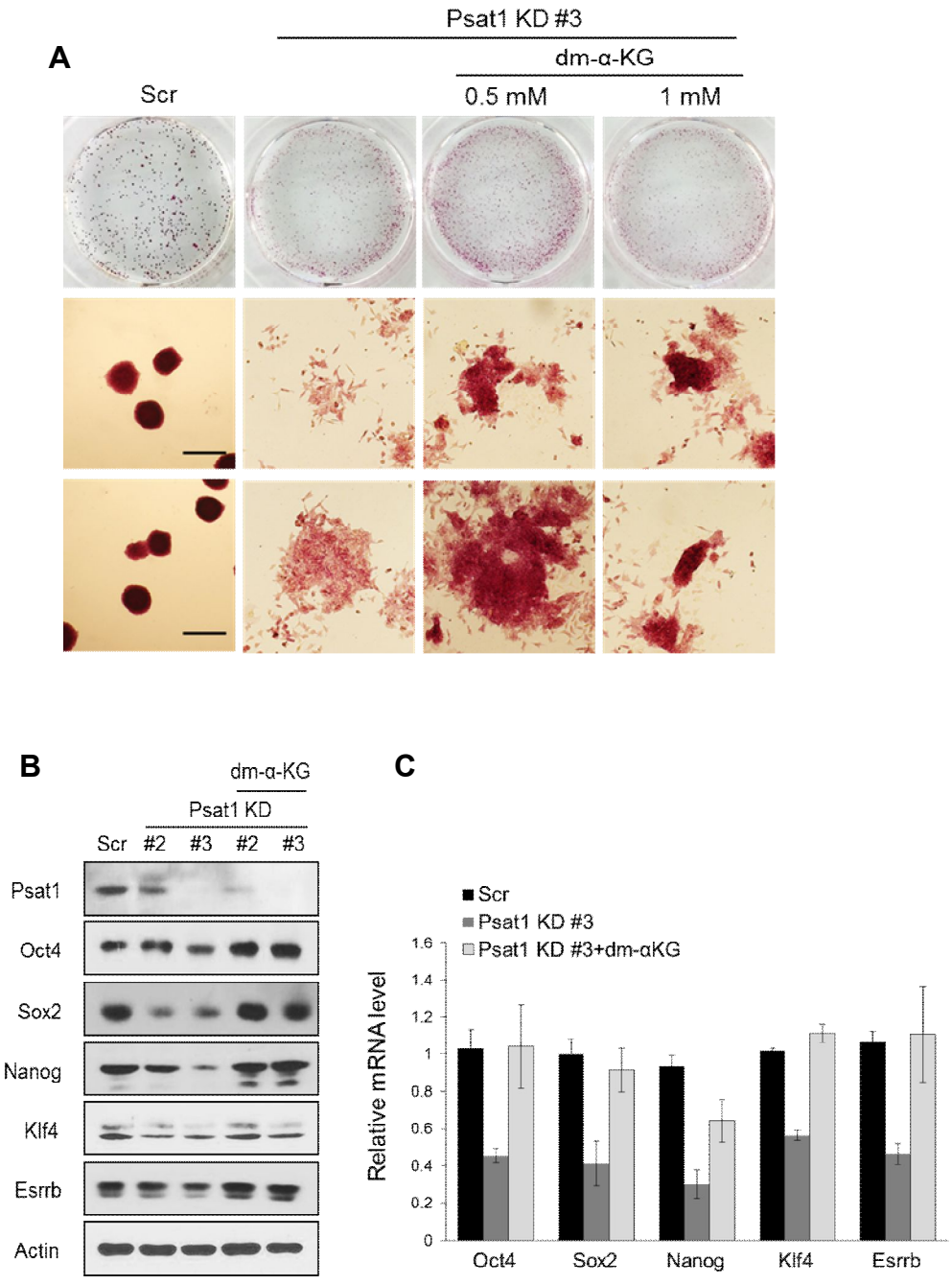
A
Psat1 KD #3
dm-α-KG
Scr
0.5 mM
1 mM
B
dm-α-KG
Psat1 KD
Scr
#2
#3
#2
#3
Psat1
Oct4
Sox2
Nanog
Klf4
Esrrb
Actin
C
Scr
Psat1 KD #3
Psat1 KD #3+dm-αKG
Relative mRNA level
1.6
1.4
1.2
1
0.8
0.6
0.4
0.2
0
Oct4
Sox2
Nanog
Klf4
Esrrb

Figure 19. Dm-α-KG treatment restores Psat1 knockdown phenotype

(A) AP staining of Psat1 knockdown clone 3 without and with dm-α-KG treatment. Differentiation was delayed when Dm-α-KG was treated. (B) Protein levels of core transcription factors in Psat1 knockdown clones 2 and 3 after dm-α-KG treatment. The protein level of core transcription factors were restored after dm-α-KG treatment (C) mRNA levels of core transcription factors in Psat1 knockdown #3 without and with dm-α-KG. * $P \leq 0.05$ ** $P \leq 0.01$ *** $P \leq 0.001$.

The up-regulation of serine *de novo* biosynthesis pathway and amplification of PHGDH altering glucose metabolism have been reported in cancers (Locasale et al., 2011; Possemato et al., 2011). Thus we examined the influence of Phgdh and Psph enzymes on pluripotency and self-renewal. knockdown of Psph, the downstream enzyme of Psat1, had no effect on mESCs, but knockdown of Phgdh, the upstream enzyme of Psat1, had partial defect in self-renewal with retarded cell proliferation (Figure 19A and 19B). Consistent with Psat1 knockdown cells, Phgdh knockdown mESCs had reduced levels of core pluripotency factors, but Psph knockdown mESCs had no such changes (Figure 19C). These results were further confirmed by tracing experiment of measuring ^{13}C incorporation into α-KG after treating [U-^{13}C]-glutamine. Fraction of incorporated ^{13}C-α-KG in Phgdh and Psat1 knockdown mESCs were decreased (Figure 20A). However, knockdown s of each of three enzymes (Phgdh, Psat1, Psph) in mESCs had reduced ^{13}C-serine level (Figure 20B), indicating that serine reduction is not critical for determining mESC state. Based on these findings and those discussed above, we suggest that Psat1 is a regulator of intracellular α-KG levels in mESCs and that sustaining Psat1 levels is crucial for maintaining pluripotency.

A

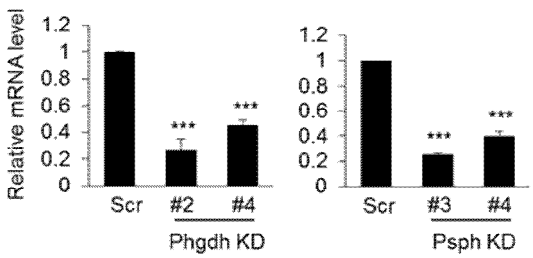
Relative mRNA level
1.2
1
0.8
0.6
0.4
0.2
0
***
***
Scr
#2
#4
Phgdh KD
***
***
Scr
#3
#4
Psph KD

B

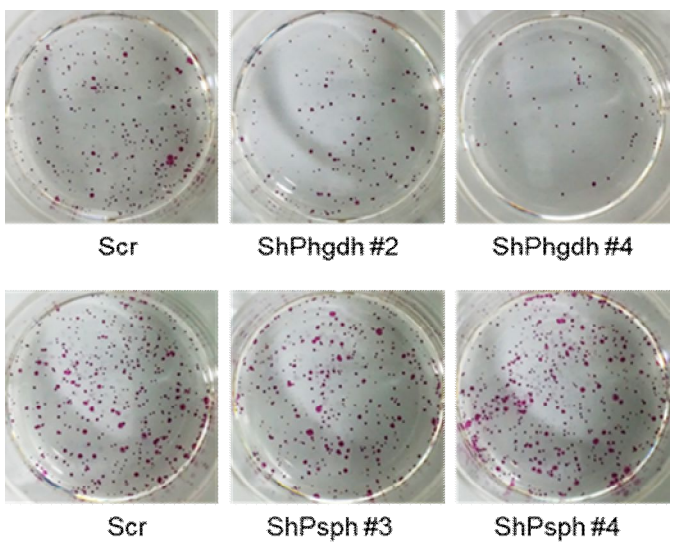
Scr
ShPhgdh #2
ShPhgdh #4
Scr
ShPsph #3
ShPsph #4

C

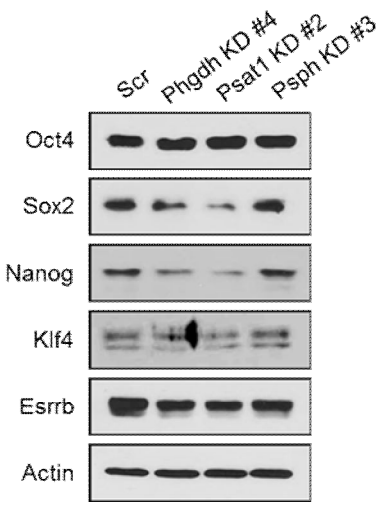
Scr
Phgdh KD #4
Psat1 KD #2
Psph KD #3
Oct4
Sox2
Nanog
Klf4
Esrrb
Actin

Figure 20. Knockdown of *de novo* serine biosynthesis enzymes

(A) shRNA mediated Phgdh and Psph knockdown levels are shown. (B) AP staining of mESCs from (A). Phgdh knockdown had reduced proliferation, but Psph knockdown had no effect on pluripotency and proliferation. (C) Protein levels of core transcription factors are shown in Scr and Phgdh, Psat1 and Psph knockdown mESCs. Psat1 and Phgdh, upstream enzyme of Psat1, had lower protein levels of core transcription factors. n=3. *** $P \leq 0.001$.

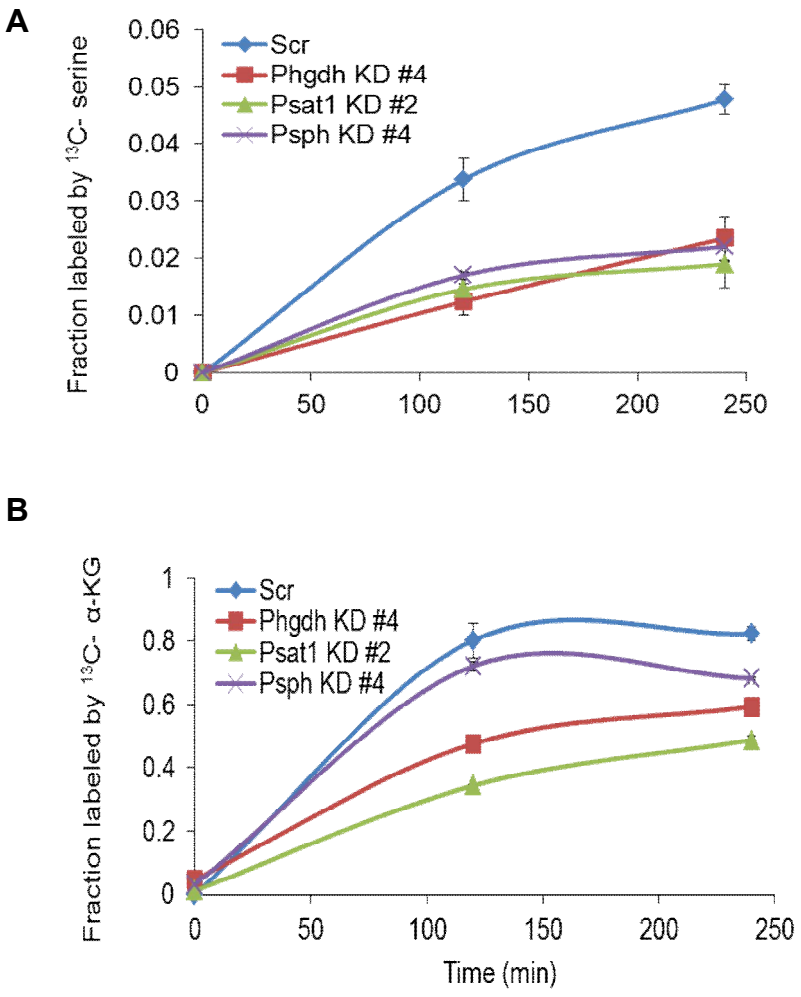

Figure 21. ^{13}C Incorporations are reduced in Psat1 knockdown mESCs

(A) Fraction of [U-^{13}C]-glucose-derived ^{13}C-serine was measured at time point of 0, 120 and 240 min (n=3). Data are presented as means ±SEM. Knockdown of all three serine biosynthesis enzymes had reduction in ^{13}C-serine (B) Fraction labeled by ^{13}C- α-KG derived from [U-^{13}C]-glutamine were compared. Psat1 and Phgdh, but not Psph, knockdown had reductino in ^{13}C- α-KG (n=3).

3-3 Psat1 Regulates Histone and DNA Methylation States in mESCs

α-KG is a cofactor of the Tet family of enzymes which catalyze conversion of 5-mC to 5'-hmC, thus we examined changes in DNA 5'-hmC in clones 1 and 2 by genomic DNA dot blot. Moderate Psat1 knockdown mESCs had lower 5'-hmC and hPsat1 rescued cells recovered 5'-hmC level (Figure 21A). Since 5'-hmC has been suggested to regulate genome-wide transcription and gene expression in stem cells (Xu et al., 2011b), we examined the enrichment of 5'-hmC on the region of core transcription factors by hydroxymethylated DNA immunoprecipitation (hMeDIP). Using publically available hMeDIP-sequencing data (Xu et al., 2011b), we found 5'-hmC-positive regions on core transcription factors were lower in Psat1 knockdown clones 1 and 2 compared to Scr cells (Figure 21B). Reduced global 5'-hmC levels were also examined in Phgdh and Psat1 knockdown mESCs (Figure 22). Next, we investigated global histone methylation changes of H3K4me3, H3K9me3, H3K27me3 and H3K36me3 in Psat1 knockdown clones 1 and 2 (Figure 23A). H3K9 methylation maintains stem cell plasticity, although its levels are usually low, and Oct4 and Nanog are targets of H3K9me3 (Loh et al., 2007). Thus we performed ChIP to verify H3K9me3 levels in Psat1 knockdown clones 1 and 2. Promoter of core transcription factors had increased H3K9me3 level compared with Scr cells (Figure 23B). Protein and mRNA levels of Tet and JHDMs were unchanged on Psat1 knockdown, indicating that these epigenetic changes occur without transcriptional alteration in these enzymes (Figure 24A and 24B).

A

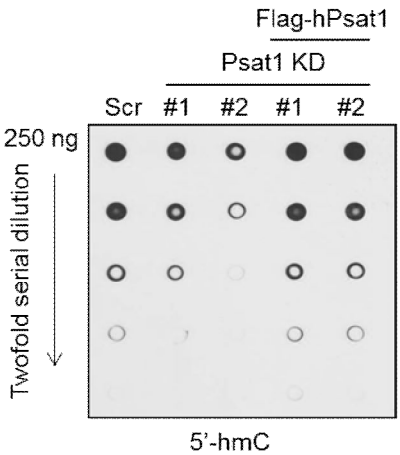
Flag-hPsat1
Psat1 KD
Scr
#1
#2
#1
#2
250 ng
Twofold serial dilution
5'-hmC

B

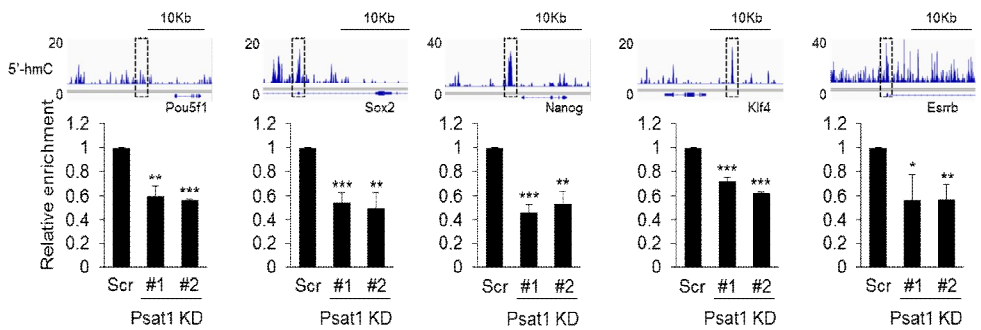
10Kb
5'-hmC
Pou5f1
Sox2
Nanog
Klf4
Esrrb
Relative enrichment
Scr
#1
#2
Psat1 KD

Figure 22. 5'-hmC level is reduced in Psat1 knockdown mESCs

(A) Dot blot analysis of genomic DNA extracted from Psat1 knockdown clones 1 and 2 and Flag-hPSAT1 rescued cell lines. Psat1 knockdown clones had decreased level of 5'-hmC (B) hMeDIP assays of core transcription factor promoter regions. 5'-hmC-positive regions (dashed box) from published hMeDIP data (top panel). Values were normalized as percentage of input and presented as relative to Scr cells. Promoter regions of core transcription factors had lowered 5'-hmC content (n=3).

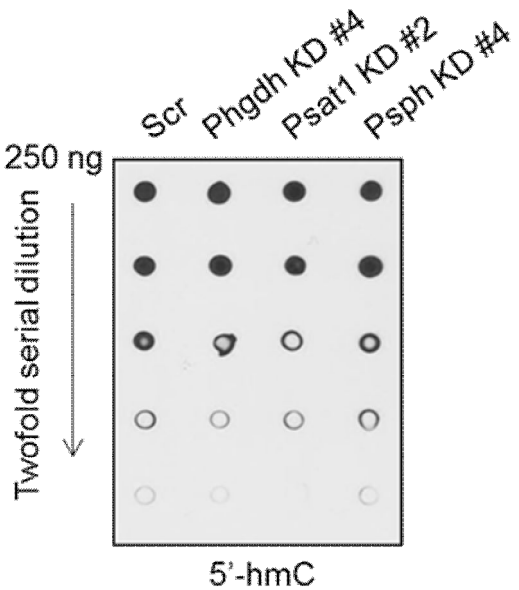

Figure 23. 5'-hmC levels in serine *de novo* biosynthesis enzymes knockdown mESCs.

Dot blot analysis of genomic DNA extracted from *de novo* serine biosynthesis enzyme knockdown mESCs. Knockdown of Phgdh Psat1, but not Psph, had reduction in 5'-hmC. Dot blots were repeated four times and the most representative data are shown.

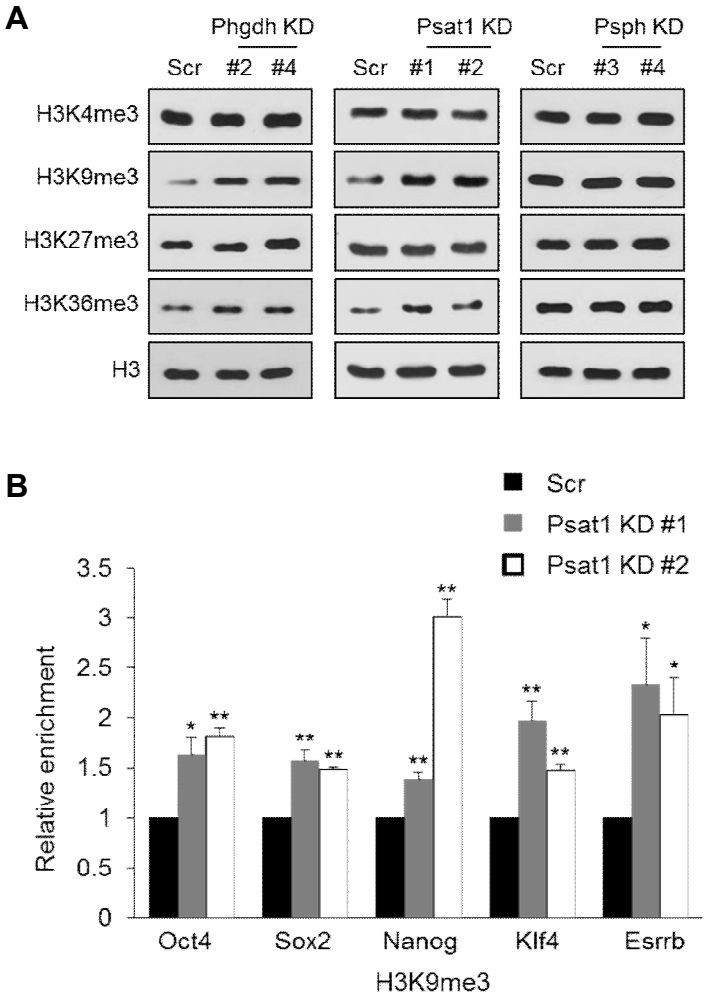

Figure 24. Methylation levels are changed in Psat1 knockdown mESCs

(A) Global histone methylation levels in *de novo* serine biosynthesis enzyme knockdown mESCs as indicated histone antibodies. (B) ChIP analysis of H3K9me3 in Psat1 knockdown cells in core transcription factor promoter regions. Values were normalized as percentage of input and presented as relative to Scr. Data are presented as means ± SEM. * $P \leq 0.05$ ** $P \leq 0.01$ *** $P \leq 0.001$.

A

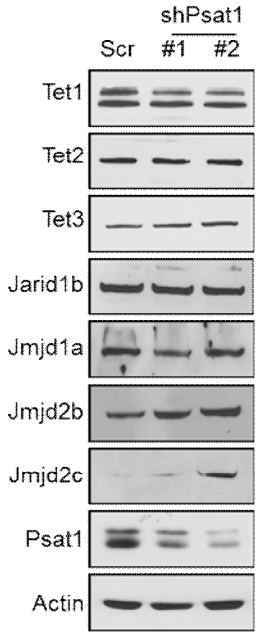
shPsat1
Scr
#1
#2
Tet1
Tet2
Tet3
Jarid1b
Jmjd1a
Jmjd2b
Jmjd2c
Psat1
Actin

B

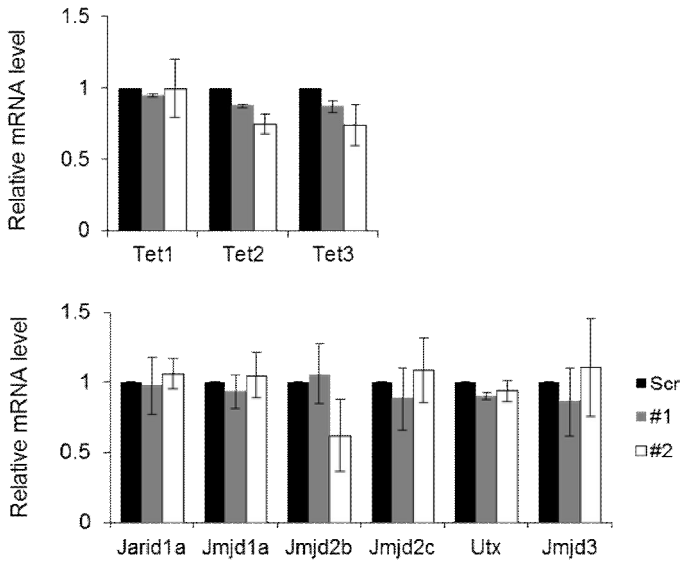
Relative mRNA level
1.5
1
0.5
0
Tet1
Tet2
Tet3
Relative mRNA level
1.5
1
0.5
0
Jarid1a
Jmjd1a
Jmjd2b
Jmjd2c
Utx
Jmjd3
Scr
#1
#2

Figure 25. Protein and mRNA levels of α-KG-dependent Tet family enzymes and JHDMs

Protein (A) and mRNA (B) levels of JHDMs and Tet family enzymes are shown by western blot and qRT-PCR assay. Psat1 knockdown clones had altered DNA and histone methylation patterns without changes in Tet and JHDM protein levels. Data are presented relative to Scr cells as means ±SEM (n=3).

Since glutamine is necessary for Psat1-catalyzing α-KG, we tested the effect of exogenous glutamine on histone methylation (Figure 25). Similar to the Psat1 knockdown, the deprivation of exogenous glutamine led to the increase of levels of H3K9me3 and H3K36me3. Moreover, up-regulation of H3K27me3 was observed without exogenous glutamine as previous paper reported (Carey et al., 2015).

Then, we determined whether increased intracellular α-KG levels also triggered epigenetic alteration. Global 5'-hmC levels rose due to dm-α-KG (Figure 26A). These results were verified by hMeDIP assay, which demonstrated increased 5'-hmC levels in the same genomic regions as in Figure 18C (Figure 26B). Global histone methylation levels after dm-α-KG treatment also affect H3K9me3, and H3K36me3 level (Figure 26C). Next, we generated stable cell lines expressing Flag-Phgdh, Flag-Psat1 and Flag-Psph to monitor increase in protein level of these enzymes could alter epigenetic states in mESCs (Figure 27A). Ectopic expression of Flag-Phgdh and Flag-Psat1 resulted in elevation of global 5'-hmC and decreased in histone H3K9me3 and H3K36me3 level (Figure 27B and 27C). Altogether, these results indicated that Psat1 level effects DNA 5'-hmC and histone methylation level changes in mESCs.

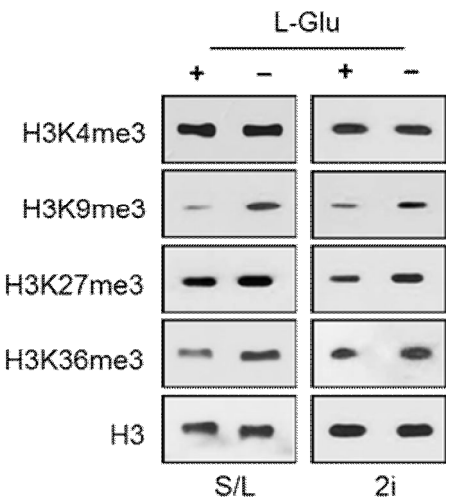

Figure 26. Histone methylation levels with and without l-glutamine

The carbon backbone of α-KG is from glutamate, supplemented in the growth medium as l-glutamine. Histone methylation levels are changed differentially depending on l-glutamine level in growth media.

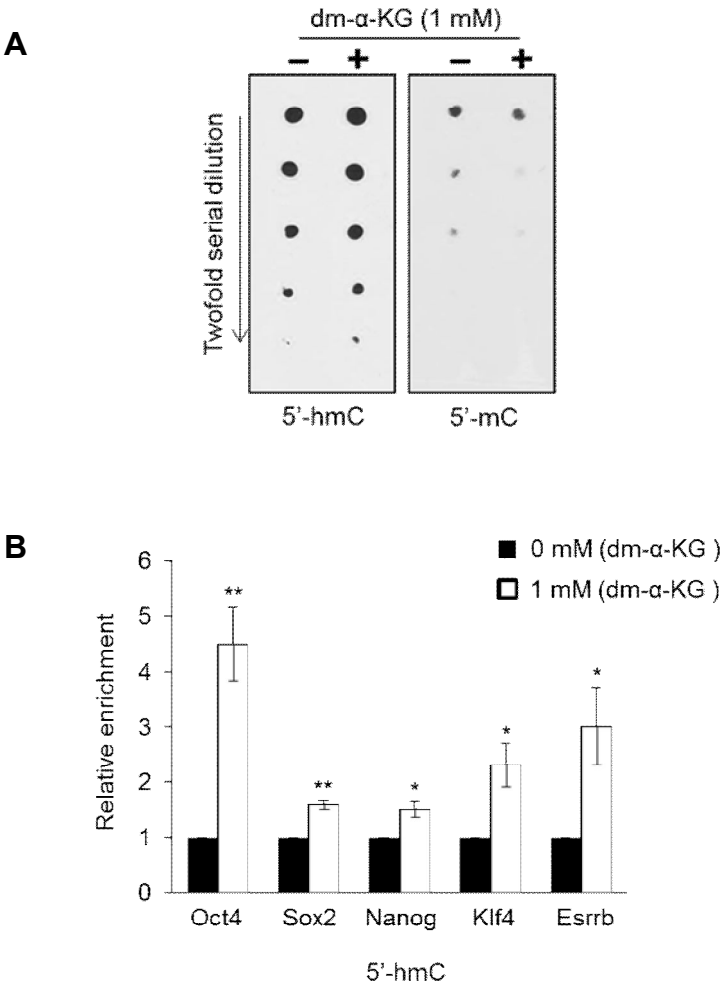
A
dm-α-KG (1 mM)
– + – +
Twofold serial dilution
5'-hmC
5'-mC
B
0 mM (dm-α-KG)
1 mM (dm-α-KG)
Relative enrichment
0
1
2
3
4
5
6
**
**
*
*
*
Oct4
Sox2
Nanog
Klf4
Esrrb
5'-hmC
C
dm-α-KG (1 mM)
– +
H3K4me3
H3K9me3
H3K27me3
H3K36me3
H3

Figure 27. Effect of dm-α-KG treatment on DNA and histone methylation

(A) Genomic DNA dot blot assay of 5'-hmC and 5'-mC after dm-α-KG treatment. Dm-α-KG treatment increased 5'-hmC content. (B) ChIP analysis of the same region in Promoter regions of core transcription factors in Figure 18B after dm-α-KG treatment of mESCs. 5'-hmC were increased (n=3). (C) Global histone methylation levels after dm-α-KG treatment. H3K9me3 and H3K36me3 were reduced. Data are presented as means ± SEM. * $P \leq 0.05$ ** $P \leq 0.01$ *** $P \leq 0.001$.

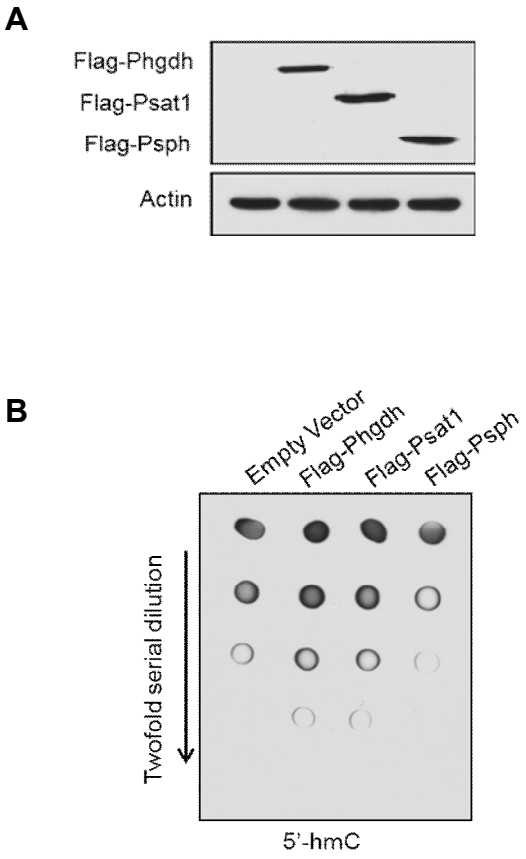
A
Flag-Phgdh
Flag-Psat1
Flag-Psph
Actin
B
Empty Vector
Flag-Phgdh
Flag-Psat1
Flag-Psph
Twofold serial dilution
5'-hmC
C
Empty Vector
Flag-Phgdh
Flag-Psat1
Flag-Psph
H3K4me3
H3K9me3
H3K27me3
H3K36me3
H3

Figure 28. Effect of ectopic expression of *de novo* serine biosynthesis enzymes

(A) Flag-Phgdh, Psat1 and Psph were ectopically expressed in mESCs. (B) Genomic DNA dot blot assay of 5'-hmC levels and (C) global histone methylation levels from mESCs in (A). Expression of Phgdh and psat1 increased 5'-hmC, but not Psph. H3K9me3 and H3K36me3 were reduced in Flag-Phgdh and Flag-Psat1 expressing clones. All the experiments is repeated at least three times.

3-4. α-KG Levels Affect the Timing of mESC Differentiation

Differentiation process coincides with the down-regulation of 5'-hmC and up-regulation of H3K9me3 (Liang and Zhang, 2013). Therefore we monitored intracellular α-KG level on spontaneous differentiation that is induced by LIF withdrawal. Notably, intracellular α-KG level was reduced gradually reaching significant degree on day 2 of LIF withdrawal (Figure 28). This prompted us to test whether perturbed α-KG reduction could affect differentiation timing. We found that dm-α-KG could not prevent mESCs from differentiating. Instead, differentiation was delayed, as evidenced by the higher portion of AP-positive colonies (Figure 29). In the pluripotent state (day 0), dm-α-KG treatment slowed the decline in core transcription factors after onset of differentiation compared with untreated mESCs (Figure 30). We treated mESCs with dm-α-KG on days 1, 2, and 3 of LIF withdrawal. Day 1 dm-α-KG-treatment had similar rates of decline with day 0, but this delayed decline did not occur in day 3 treated mESCs. Only Oct4 and Sox2 showed the delayed decline in dm-α-KG-treated cells on day 2.

Next, we examined whether lower intracellular α-KG levels by Psat1 knockdown could accelerate differentiation by measuring core transcription factors in Psat1 knockdown clone 2 after LIF withdrawal. The protein and mRNA levels of these factors decreased more rapidly in Psat1 knockdown clone 2 than in Scr cells (Figure 31A and 31B). Consistent with these data, global 5'-hmC levels declined faster in Psat1 knockdown clone 2 versus Scr cells during differentiation (Figure 32). Thus, we suggest that Psat1-mediated declines in intracellular α-KG levels determine the onset of differentiation.

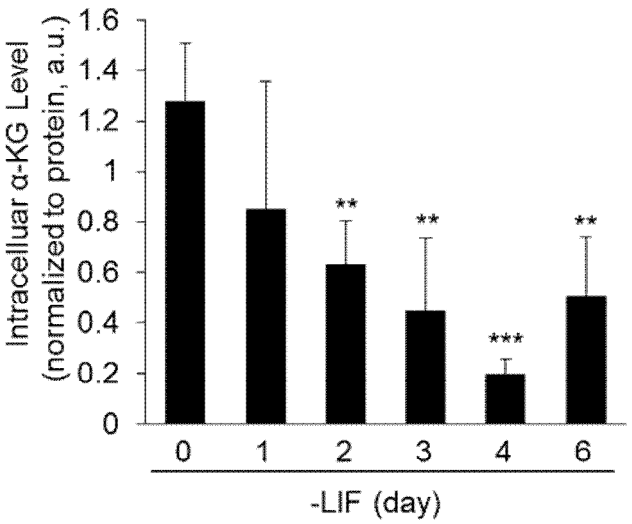

Figure 29. Intracellular α-KG level are changed during differentiation

Intracellular α-KG levels on differentiation-triggered mESCs are measured using LC-MS. α-KG level decreased gradually on subtracting LIF from culture media (n=4). ** $P \leq 0.01$ *** $P \leq 0.001$.

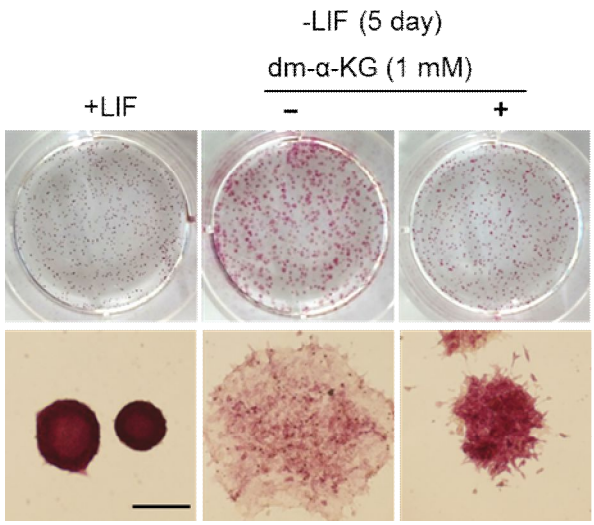

Figure 30. Dm-α-KG treatment delayed differentiation

AP staining of mESCs after 5 days of LIF removal with and without dm-α-KG. Treatment of dm-α-KG had slow progression of differentiation. This experiment is repeated three times.

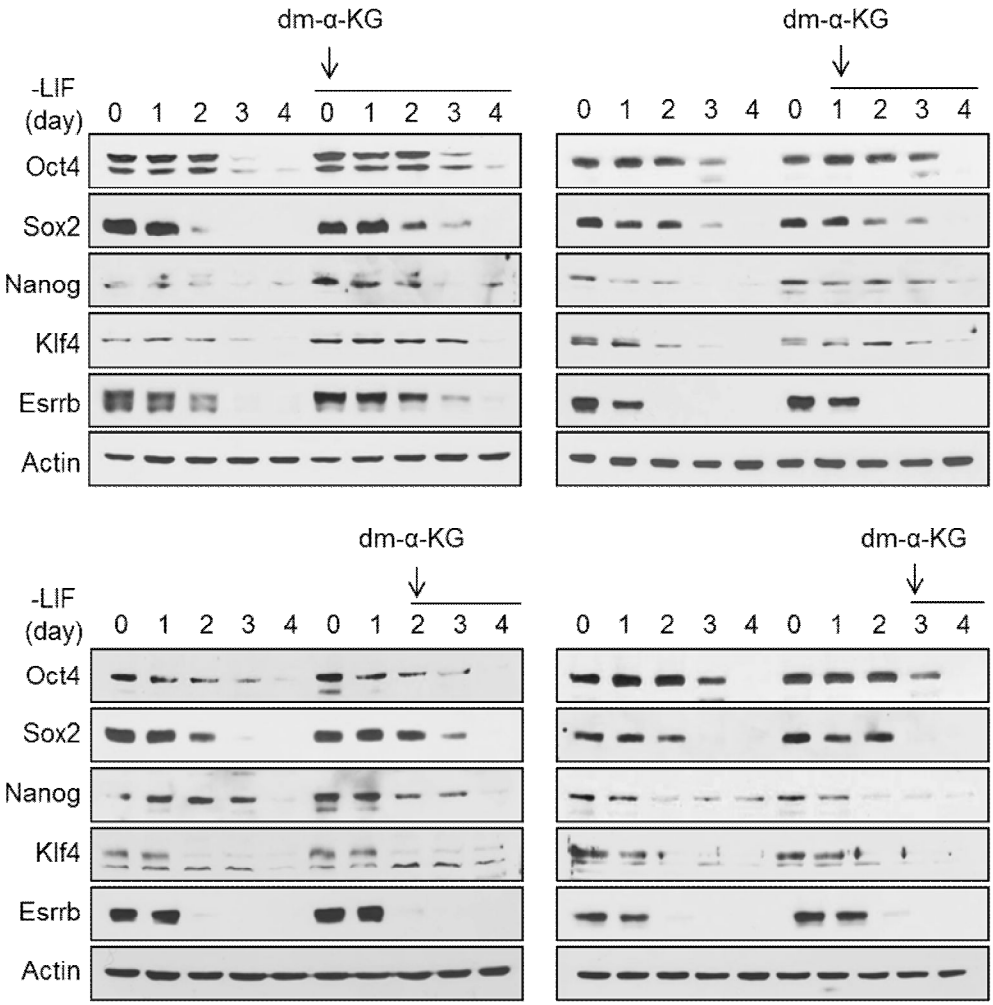
dm-α-KG
-LIF
(day)
0 1 2 3 4 0 1 2 3 4
Oct4
Sox2
Nanog
Klf4
Esrrb
Actin
dm-α-KG
0 1 2 3 4 0 1 2 3 4
dm-α-KG
-LIF
(day)
0 1 2 3 4 0 1 2 3 4
Oct4
Sox2
Nanog
Klf4
Esrrb
Actin
dm-α-KG
0 1 2 3 4 0 1 2 3 4

Figure 31. Dm-α-KG treatment delayed reduction of core transcription factors on differentiation

Western blots of differentiation-triggered mESCs on LIF withdrawal and dm-α-KG was treated on the indicated day. Disruption of intracellular α-KG on day 1 and 2 of LIF withdrawal effected the slow reduction of core transcription factors, but not in day 3 and 4 treated cells.

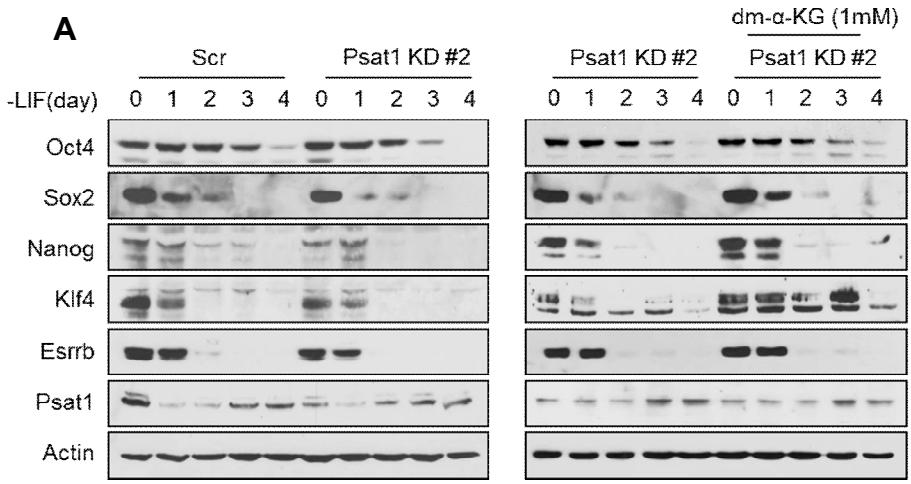
A
dm-α-KG (1mM)
Scr
Psat1 KD #2
Psat1 KD #2
Psat1 KD #2
-LIF(day)
0 1 2 3 4 0 1 2 3 4
0 1 2 3 4 0 1 2 3 4
Oct4
Sox2
Nanog
Klf4
Esrrb
Psat1
Actin

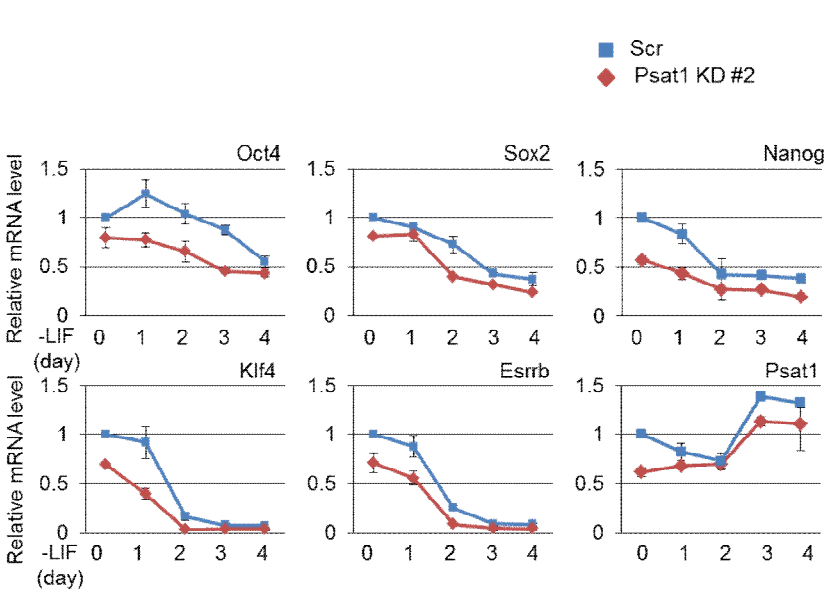
B
Scr
Psat1 KD #2
Oct4
Sox2
Nanog
Klf4
Esrrb
Psat1
Relative mRNA level
Relative mRNA level
1.5
1
0.5
0
-LIF (day)
0 1 2 3 4

Figure 32. Psat1 knockdown accelerate differentiation timing

(A) Scr and Psat1 knockdown clone 2 cells were triggered to differentiate, and core transcription factor protein levels are shown (left). Similarly, Psat1 knockdown clone 2 cells were treated with dm-α-KG, and the protein levels were compared with untreated clones (right). Psat1 knockdown clones had fast reduction rate of core transcription factors when compared to Scr clones which was recovered by treating dm- α-KG. (B) mRNA levels of core transcription factors were compared between Scr and Psat1 knockdown #2.

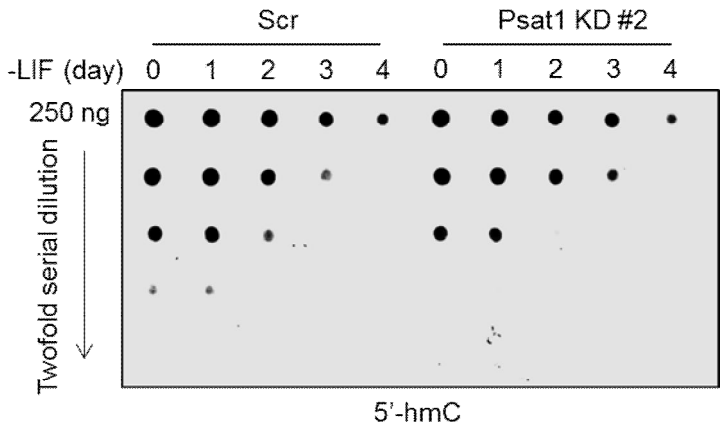

Figure 33. Psat1 knockdown mESCs had rapid reduction of 5'-hmC

Dot blot analysis showing 5'-hmC levels on LIF withdrawal in Scr and Psat1 knockdown clone 2. 5'-hmC level is reduced on differentiation and the rate was accelerated in Psat1 knockdown clones.

Since Psat1 knockdown cells have reduced level of intracellular α-KG level and thus inadequate epigenetic states, certain lineages could improperly develop due to failure of signaling and epigenetic network connection. We performed *in vivo* teratoma assay in severe combined immunodeficiency (SCID) mouse to examine if differentiation into any of three germ layers, termed endo-, meso-, ectoderm, are impaired. Injected with Psat1 knockdown clone 2 and severe Psat1 knockdown clone 3 mESCs, teratomas formed from both the Psat1 knockdown clones were smaller and weighted less compared to Scr teratomas (Figure 33A and 33B). Hematoxylin and eosin (H&E) staining of Scr cells showed differentiation into all of three germ layers (Figure 34). Teratomas from Psat1 knockdown clones 2 and 3 differentiated improperly with large portions of immature neuroectoderm and little observation of squamous epidermis and mesoderm, indicating loss of pluripotency in Psat1 knockdown mESCs (Figure 34 and Table 6).

A

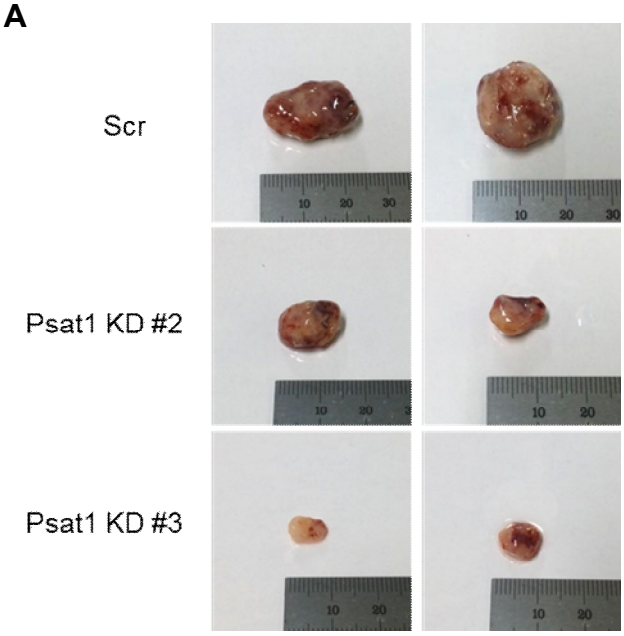

B

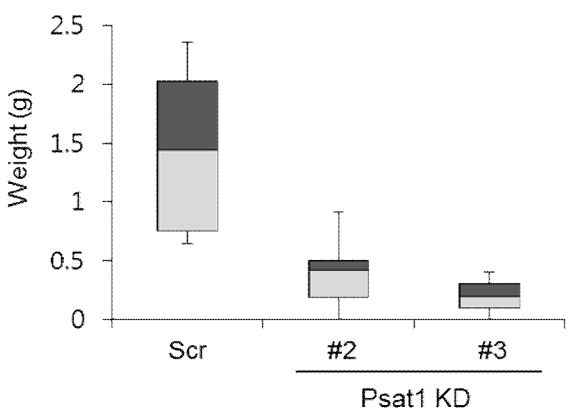

Figure 34. **Teratoma formation evaluation from Psat1 knockdown mESC transplantation**

(A) Representative photographs of teratomas dissected from SCID mouse. Teratomas dissected from SCID mouse showed that Psat1 knockdown clones had smaller or even no formation of teratomas. Graduated scale bars are in mm scale. (B) Teratomas from Scr, Psat1 knockdown clones 2 and 3 are compared in weight.

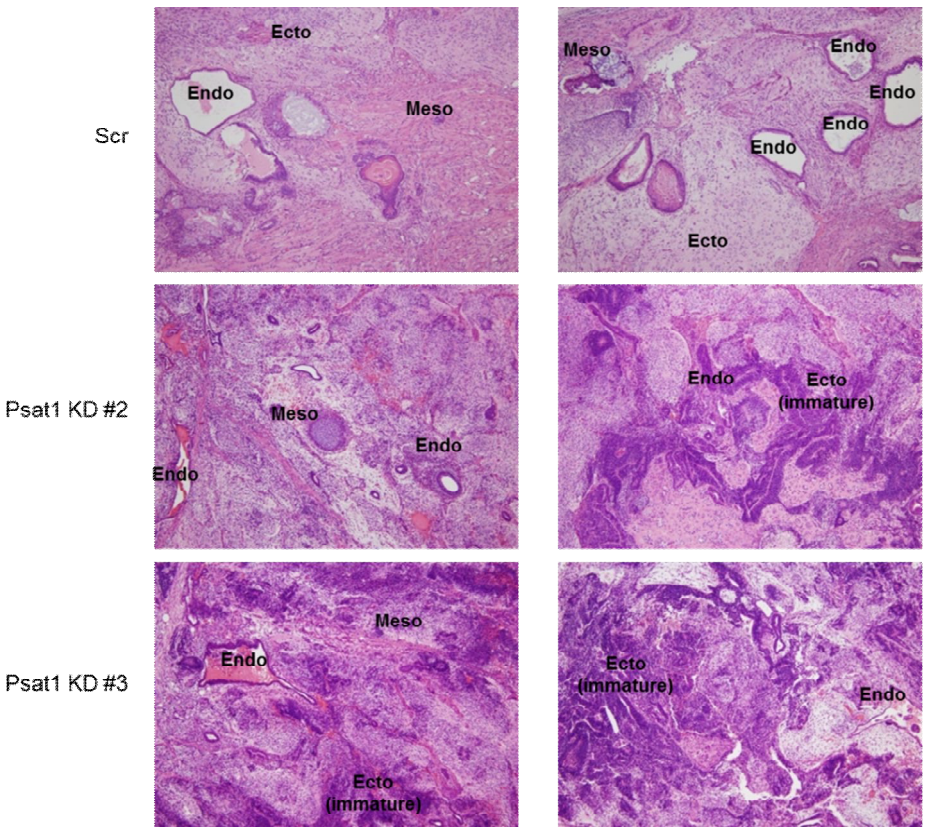

Figure 35. H&E staining of teratoma

Sections of teratomas from Scr were differentiated into three germ layers (endoderm, mesoderm and ectoderm) but, teratoma sectioning shows impaired pluripotency in Psat1 knockdown clones. Magnification x100

	Endoderm	Ecotoderm (Squamous epidermis/Neuro ectoderm)	Mesoderm
Scr	++	++ / +++	+
	++	++ / ++	+++
	+	+ / +++	+++
	++	++ / +++	++
	+	+ / +++	++
Psat1 KD #2	++	+ / +++*	++
	+	+ / +++*	++
	++	+ / +++*	++
	+	+ / ++*	+++
	+	– / +++*	–
Psat1 KD #3	+	– / +++*	–
	++	+ / +++*	++
	+	– / ++*	++
	+	– / +++*	+
	+	– / +++*	–

No observation – + ++ +++ Easy observation

Table 6. Histological analysis of teratoma sections

Sections of each teratoma were histologically analyzed with an unbiased pathologist. Most of the ectoderm in Psat1 knockdown clones was immature having a few epidermis and poor mesoderm. Asterisk indicates premature neuroectoderm.

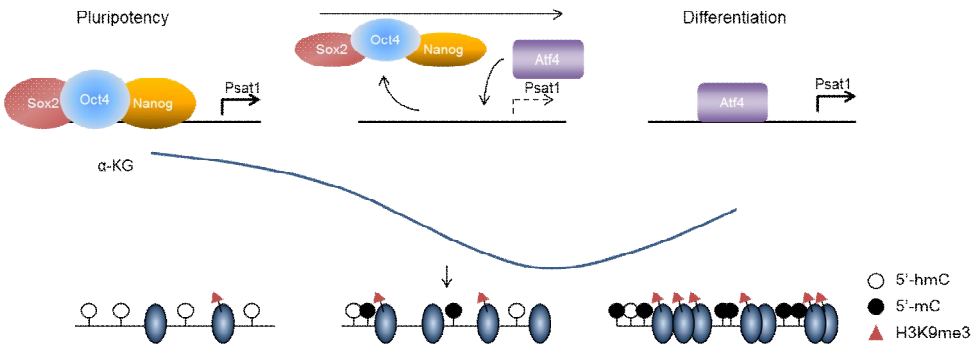

Figure 36. Schematic diagram of Psat1 function

Psat1 enhancer is occupied by OSN in pluripotent states. When differentiation triggered, OSN is released from Psat1 enhancer reducing intracellular α-KG level. The epigenetic landscape changed from high 5'-hmC to low 5'-hmC and more H3K9me3 modification on differentiation.

IV. DISCUSSION

α-KG is a key metabolite that is required for chromatin remodeling enzymes that act on histones, DNA methylation and hydroxylation of transcription factor (Loenarz and Schofield, 2011). In the middle of our study, intracellular α-KG levels were reported to promote mESC pluripotency (Carey et al., 2015). Nonetheless, the enzymes that govern the generation of α-KG and how α-KG fine-tunes the fate of mESCs with regard to maintenance and proper differentiation remain elusive. In this work, we observed that Psat1 maintains intracellular α-KG levels in mESCs and that Psat1 and α-KG levels affect the timing of differentiation. Modulation in α-KG at the onset of differentiation effects an epigenetic landscape that is amenable to differentiation (Figure 35 and 36).

De novo serine and glycine metabolism serves as feedstock for one carbon donation and deprivation of serine impaired cell growth in cancers (Jain et al., 2012; Locasale, 2013). Intriguingly, mESCs rely on threonine metabolism as SAM for methyl donor implicating that unique metabolic pathway governs mESCs to meet bioenergetics needs supporting stem cell properties (Shiraki et al., 2014; Shyh-Chang et al., 2013). Furthermore, unlike cancer cells which cannot survive under glutamine depletion (Wise and Thompson, 2010; Zhang et al., 2014), naïve mESCs can be grown without exogenous glutamine and rely on glycolysis for glutamine and α-KG supplies (Carey et al., 2015).

mESCs harbor poorly developed mitochondria, relying on glycolysis rather than oxidative phosphorylation (Xu et al., 2013; Zhang et al., 2012). Blocking glycolysis reduces the efficiency of somatic cell reprogramming, whereas enhancing glycolytic rates improves it (Folmes et al., 2011). Thus, glycolytic

metabolites that compensate for low mitochondrial metabolite content in ESCs must be identified.

With regard to Psat1-catalyzed α-KG is from the glycolysis coupling pathway, glycolysis might assume control of the epigenetic landscapes in terms of histone acetylation and DNA and histone methylation. Taken altogether, the involvement of glycolysis-branched metabolites during differentiation process seems inevitable.

In this study, intracellular α-KG led to changes in H3K9me3 and H3K36me3 levels. But, we still do not know what directs this specificity, which is likely due to the differential sensitivities of α-KG/Fe^{2+}-dependent dioxygenases on cofactors (Ozer and Bruick, 2007; Xu et al., 2011a). Interestingly, knockdown of Jmjd1a, Jmjd2b, and Jmjd2c is essential in maintaining pluripotency which are JHDMs for H3K9me3 and H3K36me3 (Das et al., 2014; Loh et al., 2007). Therefore, failed maintenance of pluripotency by severe Psat1 knockdown (clone 3) could result from the dysregulation of DNA and histone methylation. It has been referred to as that a complete defect of *Psat1* leads to early lethality (Acuna-Hidalgo et al., 2014). Thus, α-KG and Psat1 might regulate α-KG/Fe^{2+}-dependent dioxygenases *in vivo*.

Despite the major contribution of Psat1 in maintaining α-KG level in mESCs, we cannot rule out the participation of other transaminases or glutaminases since moderate Psat1 knockdown retains self-renewal states. It would be interesting to study further in terms of glutamine metabolism and mESC maintenance.

Interestingly, both glucose and glutamine availability participated in hematopoietic stem lineage specification (Oburoglu et al., 2014). Thus, Psat1-mediated production of two metabolites, glucose-derived 3-phosphoserine and

glutamine-derived α-KG could play important roles in lineage specification.

Through our study, we have demonstrated that epigenetic modifications are influenced by fluctuations in α-KG levels. By identifying Psat1 as an intracellular regulator of α-KG, we have discovered a new mechanism by which core transcription factors bridge epigenetic and metabolic changes to influence stem cell fate.

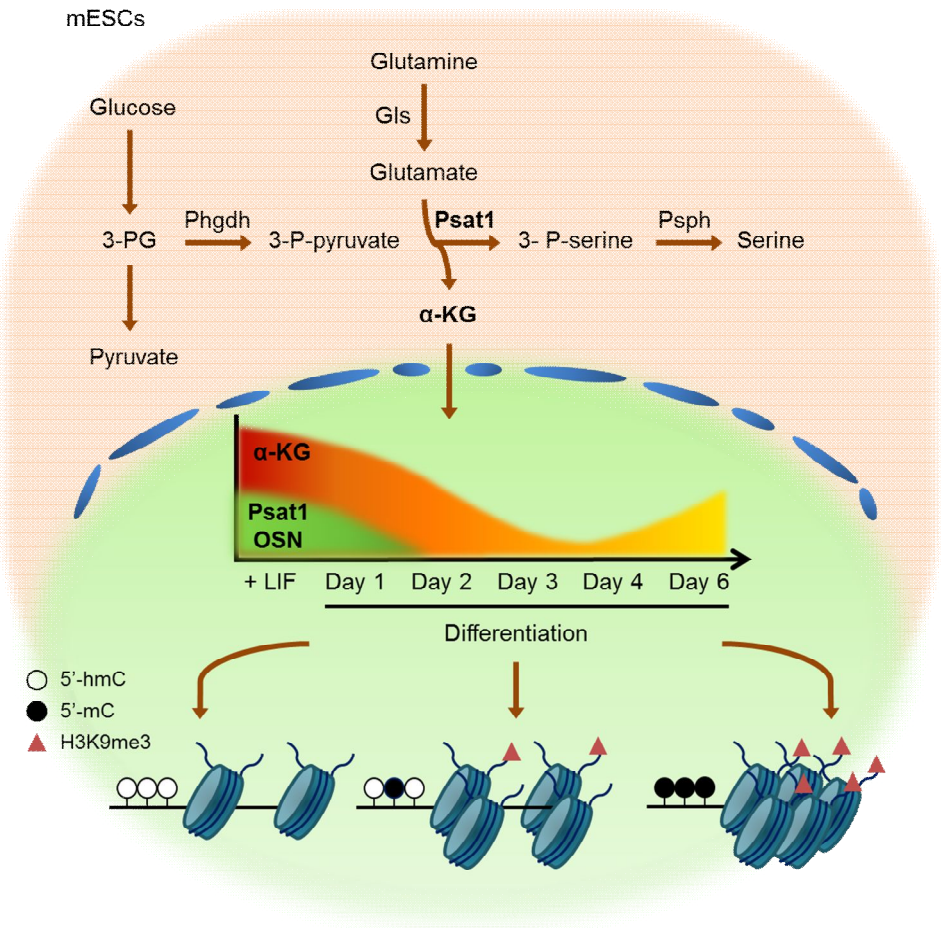

Figure 37. Graphical abstract

De novo serine biosynthesis pathway is glycolysis derived pathway. Psat1 is a second enzyme which transfers an amide group from glutamine to produce α-KG. Psat1 level is maintained by OSN in pluripotent stem cells and its level fell on differentiation and thus α-KG. α-KG is a cofactor for Tet and JHDM and predicted change the epigenetic state in ESCs.

V. REFERENCES

Acuna-Hidalgo, R., Schanze, D., Kariminejad, A., Nordgren, A., Kariminejad, M.H., Conner, P., Grigelioniene, G., Nilsson, D., Nordenskjold, M., Wedell, A., et al. (2014). Neu-Laxova syndrome is a heterogeneous metabolic disorder caused by defects in enzymes of the L-serine biosynthesis pathway. American journal of human genetics *95*, 285-293.

Carey, B.W., Finley, L.W., Cross, J.R., Allis, C.D., and Thompson, C.B. (2015). Intracellular alpha-ketoglutarate maintains the pluripotency of embryonic stem cells. Nature *518*, 413-416.

Chen, X., Xu, H., Yuan, P., Fang, F., Huss, M., Vega, V.B., Wong, E., Orlov, Y.L., Zhang, W., Jiang, J., et al. (2008). Integration of external signaling pathways with the core transcriptional network in embryonic stem cells. Cell *133*, 1106-1117.

Cimmino, L., Abdel-Wahab, O., Levine, R.L., and Aifantis, I. (2011). TET family proteins and their role in stem cell differentiation and transformation. Cell stem cell *9*, 193-204.

Das, P.P., Shao, Z., Beyaz, S., Apostolou, E., Pinello, L., De Los Angeles, A., O'Brien, K., Atsma, J.M., Fujiwara, Y., Nguyen, M., et al. (2014). Distinct and combinatorial functions of Jmjd2b/Kdm4b and Jmjd2c/Kdm4c in mouse embryonic stem cell identity. Molecular cell *53*, 32-48.

DeBerardinis, R.J., and Cheng, T. (2010). Q's next: the diverse functions of glutamine in metabolism, cell biology and cancer. Oncogene *29*, 313-324.

DeNicola, G.M., Chen, P.H., Mullarky, E., Sudderth, J.A., Hu, Z., Wu, D., Tang, H., Xie, Y., Asara, J.M., Huffman, K.E., et al. (2015). NRF2 regulates serine biosynthesis in non-small cell lung cancer. Nature genetics *47*, 1475-1481.

Folmes, C.D., Nelson, T.J., Martinez-Fernandez, A., Arrell, D.K., Lindor, J.Z., Dzeja, P.P., Ikeda, Y., Perez-Terzic, C., and Terzic, A. (2011). Somatic oxidative bioenergetics transitions into pluripotency-dependent glycolysis to facilitate nuclear reprogramming. Cell metabolism *14*, 264-271.

Galonska, C., Ziller, M.J., Karnik, R., and Meissner, A. (2015). Ground State Conditions Induce Rapid Reorganization of Core Pluripotency Factor Binding before Global Epigenetic Reprogramming. Cell stem cell *17*, 462-470.

Hwang, I.Y., Roe, J.S., Seol, J.H., Kim, H.R., Cho, E.J., and Youn, H.D. (2012). pVHL-mediated transcriptional repression of c-Myc by recruitment of histone deacetylases. Molecules and cells *33*, 195-201.

Jain, M., Nilsson, R., Sharma, S., Madhusudhan, N., Kitami, T., Souza, A.L., Kafri, R., Kirschner, M.W., Clish, C.B., and Mootha, V.K. (2012). Metabolite profiling identifies a key role for glycine in rapid cancer cell proliferation. Science *336*, 1040-1044.

Jang, H., Kim, T.W., Yoon, S., Choi, S.Y., Kang, T.W., Kim, S.Y., Kwon, Y.W., Cho, E.J., and Youn, H.D. (2012). O-GlcNAc regulates pluripotency and reprogramming by directly acting on core components of the pluripotency network. Cell stem cell *11*, 62-74.

Jixiu Shan, T.H., Tiffany A. Tang, Naohiro Terada, and Michael S. Kilberg (2013). Activation of the amino acid response modulates lineage specification during differentiation of murine embryonic stem cells. Am J Physiol Endocrinol Metab *305*, E325-E335.

Kaelin, W.G., Jr., and McKnight, S.L. (2013). Influence of metabolism on epigenetics and disease. Cell *153*, 56-69.

Klose, R.J., Kallin, E.M., and Zhang, Y. (2006). JmjC-domain-containing proteins and histone demethylation. Nature reviews. Genetics *7*, 715-727.

Lee, H.J., Hore, T.A., and Reik, W. (2014). Reprogramming the methylome: erasing memory and creating diversity. Cell stem cell *14*, 710-719.

Liang, G., and Zhang, Y. (2013). Embryonic stem cell and induced pluripotent stem cell: an epigenetic perspective. Cell research *23*, 49-69.

Locasale, J.W. (2013). Serine, glycine and one-carbon units: cancer metabolism in full circle. Nat. Rev. Cancer *13*, 572-583.

Locasale, J.W., and Cantley, L.C. (2011). Metabolic flux and the regulation of mammalian cell growth. Cell metabolism *14*, 443-451.

Locasale, J.W., Grassian, A.R., Melman, T., Lyssiotis, C.A., Mattaini, K.R., Bass, A.J., Heffron, G., Metallo, C.M., Muranen, T., Sharfi, H., et al. (2011). Phosphoglycerate dehydrogenase diverts glycolytic flux and contributes to oncogenesis. Nature genetics *43*, 869-874.

Loenarz, C., and Schofield, C.J. (2011). Physiological and biochemical aspects of hydroxylations and demethylations catalyzed by human 2-oxoglutarate oxygenases. Trends in biochemical sciences *36*, 7-18.

Loh, Y.H., Zhang, W., Chen, X., George, J., and Ng, H.H. (2007). Jmjd1a and Jmjd2c histone H3 Lys 9 demethylases regulate self-renewal in embryonic stem cells. Genes & development *21*, 2545-2557.

Marson, A., Levine, S.S., Cole, M.F., Frampton, G.M., Brambrink, T., Johnstone, S., Guenther, M.G., Johnston, W.K., Wernig, M., Newman, J., et al. (2008). Connecting microRNA genes to the core transcriptional regulatory circuitry of embryonic stem cells. Cell *134*, 521-533.

Masui, S., Nakatake, Y., Toyooka, Y., Shimosato, D., Yagi, R., Takahashi, K., Okochi, H., Okuda, A., Matoba, R., Sharov, A.A., et al. (2007). Pluripotency governed by Sox2 via regulation of Oct3/4 expression in mouse embryonic stem cells. Nature cell biology *9*, 625-635.

Mathelier, A., Zhao, X., Zhang, A.W., Parcy, F., Worsley-Hunt, R., Arenillas, D.J., Buchman, S., Chen, C.Y., Chou, A., Ienasescu, H., et al. (2014). JASPAR 2014: an extensively expanded and updated open-access database of transcription factor binding profiles. Nucleic acids research *42*, D142-147.

Mentch, S.J., Mehrmohamadi, M., Huang, L., Liu, X., Gupta, D., Mattocks, D., Gomez Padilla, P., Ables, G., Bamman, M.M., Thalacker-Mercer, A.E., et al. (2015). Histone Methylation Dynamics and Gene Regulation Occur through the Sensing of One-Carbon Metabolism. Cell metabolism *22*, 861-873.

Oburoglu, L., Tardito, S., Fritz, V., de Barros, S.C., Merida, P., Craveiro, M., Mamede, J., Cretenet, G., Mongellaz, C., An, X., et al. (2014). Glucose and glutamine metabolism regulate human hematopoietic stem cell lineage specification. Cell stem cell *15*, 169-184.

Ozer, A., and Bruick, R.K. (2007). Non-heme dioxygenases: cellular sensors and regulators jelly rolled into one? Nature chemical biology *3*, 144-153.

Possemato, R., Marks, K.M., Shaul, Y.D., Pacold, M.E., Kim, D., Birsoy, K., Sethumadhavan, S., Woo, H.K., Jang, H.G., Jha, A.K., et al. (2011). Functional genomics reveal that the serine synthesis pathway is essential in breast cancer. Nature *476*, 346-350.

Shiraki, N., Shiraki, Y., Tsuyama, T., Obata, F., Miura, M., Nagae, G., Aburatani, H., Kume, K., Endo, F., and Kume, S. (2014). Methionine metabolism regulates

maintenance and differentiation of human pluripotent stem cells. Cell metabolism *19*, 780-794.

Shyh-Chang, N., Locasale, J.W., Lyssiotis, C.A., Zheng, Y., Teo, R.Y., Ratanasirintrawoot, S., Zhang, J., Onder, T., Unternaehrer, J.J., Zhu, H., et al. (2013). Influence of threonine metabolism on S-adenosylmethionine and histone methylation. Science *339*, 222-226.

Sutendra, G., Kinnaird, A., Dromparis, P., Paulin, R., Stenson, T.H., Haromy, A., Hashimoto, K., Zhang, N., Flaim, E., and Michelakis, E.D. (2014). A nuclear pyruvate dehydrogenase complex is important for the generation of acetyl-CoA and histone acetylation. Cell *158*, 84-97.

Wamstad, J.A., Alexander, J.M., Truty, R.M., Shrikumar, A., Li, F., Eilertson, K.E., Ding, H., Wylie, J.N., Pico, A.R., Capra, J.A., et al. (2012). Dynamic and coordinated epigenetic regulation of developmental transitions in the cardiac lineage. Cell *151*, 206-220.

Wang, J., Alexander, P., Wu, L., Hammer, R., Cleaver, O., and McKnight, S.L. (2009). Dependence of mouse embryonic stem cells on threonine catabolism. Science *325*, 435-439.

Whyte, W.A., Orlando, D.A., Hnisz, D., Abraham, B.J., Lin, C.Y., Kagey, M.H., Rahl, P.B., Lee, T.I., and Young, R.A. (2013). Master transcription factors and mediator establish super-enhancers at key cell identity genes. Cell *153*, 307-319.

Wise, D.R., and Thompson, C.B. (2010). Glutamine addiction: a new therapeutic target in cancer. Trends in biochemical sciences *35*, 427-433.

Wu, J., and Izpisua Belmonte, J.C. (2015). Dynamic Pluripotent Stem Cell States and Their Applications. Cell stem cell *17*, 509-525.

Xiao, S., Xie, D., Cao, X., Yu, P., Xing, X., Chen, C.C., Musselman, M., Xie, M., West, F.D., Lewin, H.A., et al. (2012). Comparative epigenomic annotation of regulatory DNA. Cell *149*, 1381-1392.

Xu, W., Yang, H., Liu, Y., Yang, Y., Wang, P., Kim, S.H., Ito, S., Yang, C., Wang, P., Xiao, M.T., et al. (2011a). Oncometabolite 2-hydroxyglutarate is a competitive inhibitor of alpha-ketoglutarate-dependent dioxygenases. Cancer cell *19*, 17-30.

Xu, X., Duan, S., Yi, F., Ocampo, A., Liu, G.H., and Izpisua Belmonte, J.C. (2013). Mitochondrial regulation in pluripotent stem cells. Cell metabolism *18*, 325-332.

Xu, Y., Wu, F., Tan, L., Kong, L., Xiong, L., Deng, J., Barbera, A.J., Zheng, L., Zhang, H., Huang, S., et al. (2011b). Genome-wide regulation of 5hmC, 5mC, and gene expression by Tet1 hydroxylase in mouse embryonic stem cells. Molecular cell *42*, 451-464.

Ye, J., Mancuso, A., Tong, X., Ward, P.S., Fan, J., Rabinowitz, J.D., and Thompson, C.B. (2012). Pyruvate kinase M2 promotes de novo serine synthesis to

sustain mTORC1 activity and cell proliferation. Proceedings of the National Academy of Sciences of the United States of America *109*, 6904-6909.

Yun, J., Johnson, J.L., Hanigan, C.L., and Locasale, J.W. (2012). Interactions between epigenetics and metabolism in cancers. Front. Oncol. *2*, 163.

Zhang, J., Fan, J., Venneti, S., Cross, J.R., Takagi, T., Bhinder, B., Djaballah, H., Kanai, M., Cheng, E.H., Judkins, A.R., et al. (2014). Asparagine plays a critical role in regulating cellular adaptation to glutamine depletion. Mol Cell *56*, 205-218.

Zhang, J., Nuebel, E., Daley, G.Q., Koehler, C.M., and Teitell, M.A. (2012). Metabolic regulation in pluripotent stem cells during reprogramming and self-renewal. Cell stem cell *11*, 589-595.

Ⅵ. ABSTRACT IN KOREAN

국문 초록

Phosphoserine aminotransferase-1에의한 α-ketoglutarate 조절이 배아줄기세포 분화 시기에 끼치는 영향

황 인 영

줄기세포가 분화하여 하나의 개체를 형성하는 과정에서 후생유전학적인 변화와 대사 변화가 수반되어 일어난다. 줄기세포 특성 유지와 분화 조절에 가장 중요한 이 두 기작은 상호 조절 될 것이라 사료되나 이에 대한 연구는 미비한 수준이다. 본 연구는 Phosphoserine aminostransferase 1(Psat1) 효소가 전분화성 유지 필수 전사 인자인 Oct4, Sox2 그리고 Nanog의 타겟 유전자 일 뿐만 아니라 대사 물질인 α-KG를 조절하고, 이를 통하여 줄기세포 운명을 결정한다는 사실을 증명하였다. Psat1은 줄기세포의 전분화성 유지와 자기복제에 필수 적이며, Psat1의 변화는 α-KG 레벨변화를 야기하고 이는 줄기세포 후생유전학적인 변화를 일으켰다. Psat1의 감소와 α-KG 감소는 DNA 5'-hydroxylmethylation과 감소와 histone demethylation 증가를, α-KG 증가는 DNA 5'-hydroxylmethylation의 증가와 histone methylation 감소를 일으켰다. 초기 줄기세포 분화 시 세포 내에 α-KG 변화가 일어남을 확인 할 수 있었는데, α-KG 감소를 억제하는 것은 줄기세포 분화 시기에 영향을 끼쳤다. 더 나아가 Psat1 은 ectodermal lineage로의 분화를 유도하는데 필수적임을 확인하였다. 따라서 Psat1에 의한 α

-KG 조절은 대사와 후생유전학적인 변화가 어떻게 상호 조절되어 줄기세포 운명을 결정하는지를 밝히는 중요한 연구라 사료된다.

주요어: 줄기세포, 대사, 후생유전학, Phosphoserine aminotransferase-1, α-ketoglutarate

학번: 2009-21911